

# Lawrence Berkeley National Laboratory

## Recent Work

### Title

Photocatalytic Production of Hydrogen Peroxide over Modified Semiconductor Materials:  
A Minireview

### Permalink

<https://escholarship.org/uc/item/42g0j8jm>

### Journal

Topics in Catalysis, 63(9-10)

### ISSN

1022-5528

### Authors

Song, H  
Wei, L  
Chen, L  
et al.

### Publication Date

2020-09-01

### DOI

10.1007/s11244-020-01317-9

Peer reviewed

# Photocatalytic production of hydrogen peroxide over modified semiconductor materials:

## A minireview

Haiyan Song<sup>a</sup>, Lishan Wei<sup>a</sup>, Luning Chen<sup>b</sup>, Han Zhang<sup>a,\*</sup>, Ji Su<sup>b,\*</sup>

<sup>a</sup> Department of Chemistry and Chemical Engineering, College of Chemistry, Chemical Engineering and Resource Utilization, Northeast Forestry University, Harbin, 150040, P. R. China

<sup>b</sup> Materials Sciences Division, Lawrence Berkeley National Laboratory, Berkeley, California 94720, United States.

Corresponding author:

### **Han Zhang**

Phone: +86-451-8219-0679

E-mail: [Zhanghantdcq@126.com](mailto:Zhanghantdcq@126.com)

### **Ji Su**

Phone: +1-(510) 486-4829

E-mail: [jisu@lbl.gov](mailto:jisu@lbl.gov)

Email:

Haiyan Song, [chem\\_shy@163.com](mailto:chem_shy@163.com)

Lishan Wei, [Weilishandddct5439@126.com](mailto:Weilishandddct5439@126.com)

Han Zhang, [Zhanghantdcq@126.com](mailto:Zhanghantdcq@126.com)

**Abstract:** Hydrogen peroxide ( $\text{H}_2\text{O}_2$ ) has exhibited huge application value in many fields including chemical synthesis, medicine, environmental remediation, and fuel cells. Traditional anthraquinone method for  $\text{H}_2\text{O}_2$  commercial production has emerged the drawbacks of toxicity,  $\text{H}_2$  consumption and high energy input. Photocatalytic production of  $\text{H}_2\text{O}_2$ , which only requires water, oxygen, solar light and catalyst, is a novel and green technique, and potentially becomes one of the substitutes for anthraquinone method. Herein, we comprehensively review the research progress in the reported semiconductor catalysts, their modification strategies, as well as the related photocatalysis systems and mechanisms for the light driven  $\text{H}_2\text{O}_2$  production. In detail, the photocatalysts are introduced from different families including ZnO, g- $\text{C}_3\text{N}_4$ ,  $\text{TiO}_2$ , metal complexes, metal sulfides, Bi containing semiconductors, and carbon materials. In the meantime, their modification strategies are systematically evaluated aiming at the improvement in the structures and the photoelectrical properties of semiconductors, as well as their effective activation of molecular  $\text{O}_2$ , and inhibition of  $\text{H}_2\text{O}_2$  decomposition. Finally, this review is concluded with a brief summary and outlook, and the major challenges for the development of photocatalytic  $\text{H}_2\text{O}_2$  production over the emerging semiconductor photocatalysts. ~~This review is expected to provide a theoretical and understanding foundation for the development of photocatalytic  $\text{H}_2\text{O}_2$  production.~~

**Keywords:** Hydrogen peroxide; Photocatalysis; Oxygen reduction; Semiconductors; Modification.

## 1. Introduction

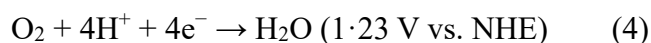
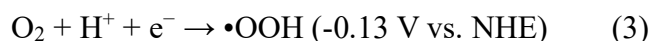
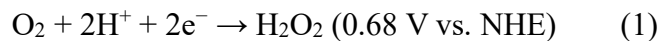
Hydrogen peroxide ( $\text{H}_2\text{O}_2$ ) is a green and efficient oxidant, which can oxidize various inorganic and organic substrates in liquid-phase reactions under very mild conditions, and generates only one clean byproduct of water ( $\text{H}_2\text{O}$ ).  $\text{H}_2\text{O}_2$  has been widely used in ~~almost all~~ many industrial fields including chemical industry, medicine and biological process, and environmental remediation [1, 2]. Very recently,  $\text{H}_2\text{O}_2$  is also exploited to be a potential energy carrier for fuel cells [3-5].  $\text{H}_2\text{O}_2$  exhibits several advantages to become an alternative to  $\text{H}_2$  fuel cells: 1)  $\text{H}_2\text{O}$  is the only and clean byproduct in fuel cells; 2) the liquid state of  $\text{H}_2\text{O}_2$  makes it more convenient and safer in storage and transportation; 3) it can be made into a fuel cell of single-compartment with more simplification and better scales than that of  $\text{H}_2$  two-compartment.

$\text{H}_2\text{O}_2$  production of industrial scale has been achieved via the anthraquinone oxidation (AO) process [6, 7]. However, anthraquinone oxidation is a multistep method that contains hydrogenation, oxidation and extraction procedures in organic solvents, requiring high energy input and emitting a lot of wastes [7, 8]. Therefore, the AO method aggravates the difficulty and hazards in transport and storage, and hardly satisfies the demands for green production and the cost efficiency. Other alternative methods, such as alcohol oxidation and electrochemical synthesis have also been ~~are also~~ practiced in industrial production of  $\text{H}_2\text{O}_2$  [6, 8, 9]. However, the purity and quality of the produced  $\text{H}_2\text{O}_2$  via those methods is not as good as ~~the two methods are worse than~~ that via the AO process. Therefore, it is essential to develop cost-effective and eco-friendly methods for  $\text{H}_2\text{O}_2$  production. During the last two decades, direct synthesis of  $\text{H}_2\text{O}_2$  from hydrogen ( $\text{H}_2$ ) and oxygen ( $\text{O}_2$ ) in the presence of a catalyst has been regarded as another alternative approach for AO process [10-14]. The direct method is an

innovation that  $\text{H}_2\text{O}_2$  is simply synthesized from its elements by one step, and the  $\text{H}_2\text{O}_2$  can be used in an oxidation reaction in situ. There are three major problems for the direct method: 1) inert gas (e.g.  $\text{N}_2$ ,  $\text{CO}_2$  and Ar) must be charged in order to keep away from the explosive limit of  $\text{H}_2/\text{O}_2$  mixture; 2) the noble metals (e.g. Pd, Au and Pt), and their alloys (e.g. Pd-Au and Pd-Pt) act as the active centers on various supports, which increase the cost of catalyst; 3) some noble metals like Pd and Au are also active for the  $\text{H}_2\text{O}_2$  decomposition, which decreases the synthesis efficiency of  $\text{H}_2\text{O}_2$   ~~$\text{H}_2\text{O}_2$  selectivity~~. Although the catalytic oxidation of  $\text{H}_2$  to generate  $\text{H}_2\text{O}_2$  has been known since 1914, this technique has not yet been put into industrial practice [15].

In recent years,  $\text{H}_2\text{O}_2$  production from photocatalysis of semiconductors arouses much attention and is frequently reported due to the sufficient and renewable sunlight as driving force [16]. Photocatalytic production of  $\text{H}_2\text{O}_2$  over semiconductor is at least known since the report of Baur and Neuweiler in 1927 [17]. This developing technique involves only light, water, molecular  $\text{O}_2$  and the catalyst, which is eco-friendly, and is recommended to be applied in the field of oxidations and solar fuels demanding for a mild scale of  $\text{H}_2\text{O}_2$ . In general, the photocatalysis process involves two major half reactions: 1) two-electron reduction of  $\text{O}_2$  from the conduction band (CB) (Eq. 1); 2) oxidation of  $\text{H}_2\text{O}$  by holes ( $\text{h}^+$ ) in valence band (VB) to generate  $\text{O}_2$  (Eq. 2). Meanwhile, there are several side reactions, which lower the  $\text{H}_2\text{O}_2$  selectivity: 1) one-electron reduction of  $\text{O}_2$  to generate peroxy radicals ~~superoxide radical~~ ( $\bullet\text{OOH}$ ) (Eq. 3); 2) four-electron reduction of  $\text{O}_2$  to generate  $\text{H}_2\text{O}$  (Eq. 4). Therefore,  $\text{H}_2\text{O}_2$  concentrations in many reported works hardly achieve the mmol/L scale due to the existence of those side reactions. ~~Therefore, the side reactions result in the unsatisfactory  $\text{H}_2\text{O}_2$~~

~~concentration, which hardly achieve the mmol/L scale in many reported works.~~ In the field of photocatalytic production of H<sub>2</sub>O<sub>2</sub>, effective inhibition of the one-electron and the four-electron reductions of O<sub>2</sub> becomes the major challenge for most of the semiconductor photocatalysts. Introducing the new structures or the guest molecules to the host semiconductors is an effective ~~strategy option~~ to promote the charge separation and increase the selectivity of the two-electron reduction of O<sub>2</sub> to H<sub>2</sub>O<sub>2</sub>. In addition, multi-channels for H<sub>2</sub>O<sub>2</sub> production are possibly opened by the modified semiconductors. In another aspect, a number of works adopt molecular O<sub>2</sub> (pure oxygen gas) or organic electron donors (alcohols) to enhance the H<sub>2</sub>O<sub>2</sub> yield, which are far away from the concept of cost-efficiency and green synthesis. Therefore, saving the pure O<sub>2</sub> or electron donor by using appropriate photocatalyst becomes another challenge for photocatalytic production of H<sub>2</sub>O<sub>2</sub>.



So far, the reported catalysts for photocatalytic production of H<sub>2</sub>O<sub>2</sub> can be classified as graphitic carbon nitride (g-C<sub>3</sub>N<sub>4</sub>) [16, 18-28], TiO<sub>2</sub> [29-34], transition metal sulfide [35-39], BiVO<sub>4</sub> [40], transition metal complexes [41-45] and organic ions [46, 47] based materials. In this minireview, we mainly aim at the recent advances and challenges associated with the photocatalytic H<sub>2</sub>O<sub>2</sub> production, as well as the related semiconductor photocatalysts. It contains the preparation of semiconductors, the modification strategies, and the related mechanism of H<sub>2</sub>O<sub>2</sub> production over the semiconductors.

## 2. Photocatalytic production of H<sub>2</sub>O<sub>2</sub> over g-C<sub>3</sub>N<sub>4</sub> based materials

So far, the reports on g-C<sub>3</sub>N<sub>4</sub> as fundamental catalysts for light-driven H<sub>2</sub>O<sub>2</sub> production are rapidly increasing in number. G-C<sub>3</sub>N<sub>4</sub>, consisting of earth-abundant elements only, and possessing 2.7 eV of band gap and graphene-like 2D morphology, has been regarded as an appealing and potential photocatalyst. The conduction band of g-C<sub>3</sub>N<sub>4</sub> (-1.3 V vs. NHE) is suitably located to facilitate O<sub>2</sub> reduction (-0.28 V vs. NHE), and its lower valence band potential (1.4 V vs. NHE) can prevent the oxidative decomposition of H<sub>2</sub>O<sub>2</sub>. Many efforts have been made for g-C<sub>3</sub>N<sub>4</sub> to solve the problems ~~that~~ of the fast charge recombination caused intrinsically by the  $\pi$ - $\pi$  conjugated electronic system of g-C<sub>3</sub>N<sub>4</sub> framework, and the limited inhibition of the one-electron reduction of O<sub>2</sub>.

### 2.1. Single C<sub>3</sub>N<sub>4</sub> photocatalysts

Fabrication of a single C<sub>3</sub>N<sub>4</sub> photocatalyst is a simple and low-cost way to enhance ~~to enhanced~~ the photocatalytic performance. The single C<sub>3</sub>N<sub>4</sub> photocatalyst can be fabricated based on the preparation of pristine g-C<sub>3</sub>N<sub>4</sub> without adding or doping other species. After the treatments of instruments or chemical reagents, the photocatalysts can achieve the improvements in their frameworks, pores and surface, crystal structure, or photoelectric properties to increase the H<sub>2</sub>O<sub>2</sub> productivity.

One of the strategies is to fabricate the g-C<sub>3</sub>N<sub>4</sub> of appropriate morphology without changing its intrinsic molecule or crystal structure. Shiraishi et al. earlier used the metal-free polymeric photocatalyst g-C<sub>3</sub>N<sub>4</sub> for photocatalytic production of H<sub>2</sub>O<sub>2</sub> (Fig. 1 a) [21, 48]. They found that g-C<sub>3</sub>N<sub>4</sub> with alcohol and O<sub>2</sub> can selectively promote the two-electron reduction of O<sub>2</sub> due to the efficient formation of 1,4-endoperoxide species on its surface, while suppressed the subsequent

decomposition of the formed  $\text{H}_2\text{O}_2$ . In addition, the  $\text{g-C}_3\text{N}_4$  catalyst activated by visible light can oxidize water owing to the positively shifted VB levels, while maintaining high selectivity for two-electron reduction of  $\text{O}_2$ . This thus facilitated highly efficient production of  $\text{H}_2\text{O}_2$  with more than 90% selectivity. In order to improve the catalytic activity and the  $\text{H}_2\text{O}_2$  selectivity of  $\text{g-C}_3\text{N}_4$ , the same group subsequently reported a mesoporous  $\text{g-C}_3\text{N}_4$  prepared by silica-templated thermal polymerization of cyanamide for photocatalytic production of  $\text{H}_2\text{O}_2$  [26]. Mesoporous  $\text{g-C}_3\text{N}_4$  with larger surface area contained primary amine groups on the surface, which decreased the  $\text{H}_2\text{O}_2$  selectivity and increased the photocatalytic decomposition of the formed  $\text{H}_2\text{O}_2$ . Selectivity for  $\text{H}_2\text{O}_2$  formation via two-electron reduction of  $\text{O}_2$  by the conduction band electrons localized on the 1,4-positions of the melem unit decreased with an increase in the surface area. Therefore,  $\text{H}_2\text{O}_2$  productivity was adjusted by the surface area and the surface defects of mesoporous  $\text{g-C}_3\text{N}_4$  (Fig. 1 b-d) (Fig. 1 b, e). Ou et al. developed a self-assembly method to prepare a self-supported  $\text{C}_3\text{N}_4$  aerogel with large surface area, incorporated functional groups and 3D network structure [49]. The  $\text{C}_3\text{N}_4$  aerogel obtained high photocatalytic activity for hydrogen evolution and  $\text{H}_2\text{O}_2$  photoproduction.



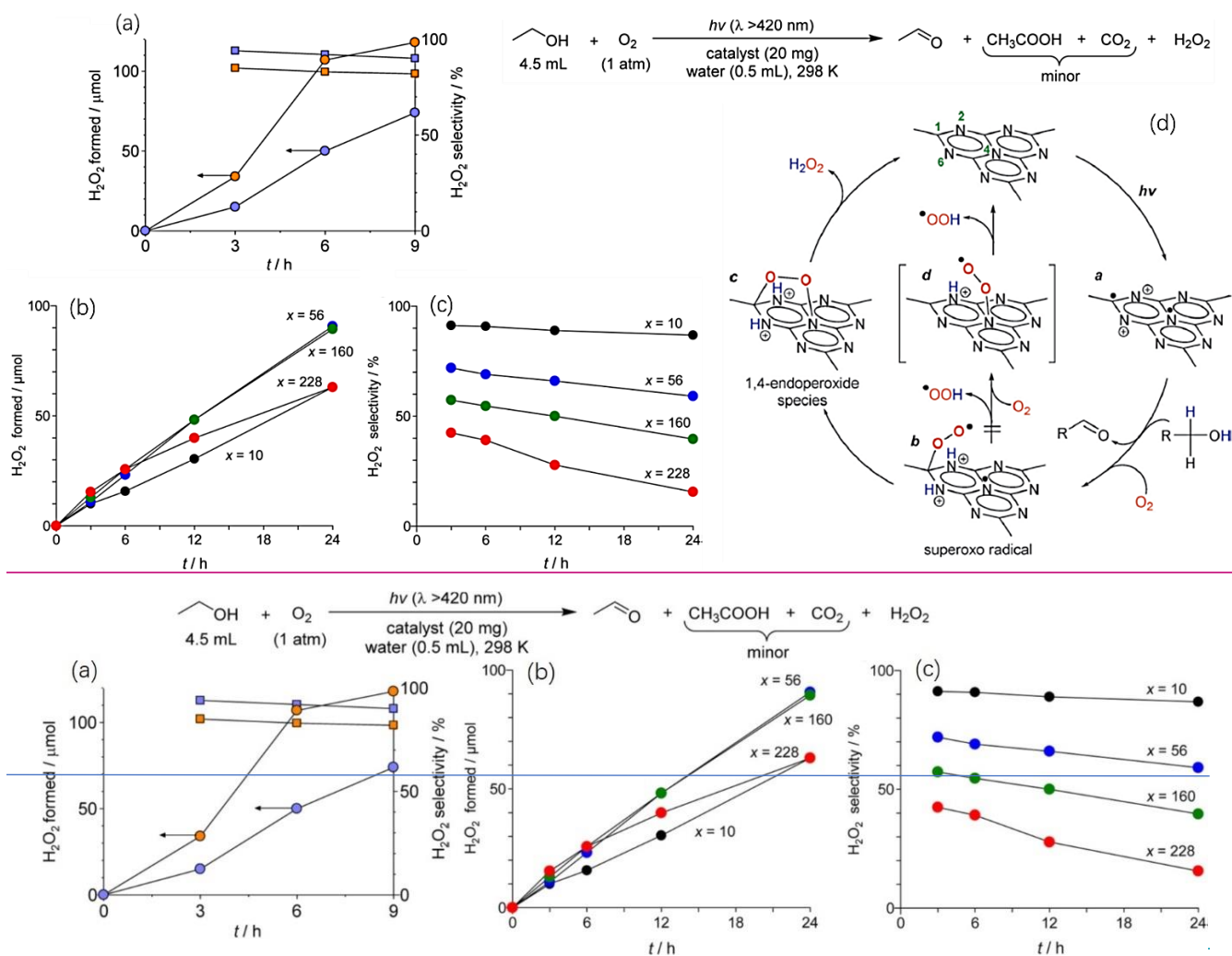


Fig.1. Amount and selectivity of H<sub>2</sub>O<sub>2</sub> over g-C<sub>3</sub>N<sub>4</sub> in a 2-propanol/water/O<sub>2</sub> system under

sunlight exposure (orange) without filter and (blue) with filter (λ > 420 nm) (a) [21].

copyright 2014 American Chemical Society; amount (b) and selectivity (c) of H<sub>2</sub>O<sub>2</sub> over

mesoporous g-C<sub>3</sub>N<sub>4</sub> with different surfaces areas (x, m<sup>2</sup> g<sup>-1</sup>) [26]. copyright 2015 American

Chemical Society; pathway of selective H<sub>2</sub>O<sub>2</sub> production on g-C<sub>3</sub>N<sub>4</sub> under visible light

irradiation (d) [26]. copyright 2015 American Chemical Society.

Another strategy is to improve the photoelectric properties of g-C<sub>3</sub>N<sub>4</sub> by introduction of vacancies or displacement of atoms. Carbon vacancies method was adopted to modulate g-C<sub>3</sub>N<sub>4</sub> with an improvement in electrons transfer and band gap Zhu et al. adopted carbon vacancies method to modulate g-C<sub>3</sub>N<sub>4</sub> with an improvement in electrons transfer and band gap [50]. H<sub>2</sub>O<sub>2</sub>

generation pathway could be changed from a two-step single-electron indirect reduction to the one-step two-electron direct reduction by the carbon vacancies in g-C<sub>3</sub>N<sub>4</sub>. Therefore, photoproduction of H<sub>2</sub>O<sub>2</sub> was improved by 14 times in the absence of organic scavenger through the carbon vacancy-based strategy. A reduced g-C<sub>3</sub>N<sub>4</sub> material was prepared by a thermal treatment with NaBH<sub>4</sub> in N<sub>2</sub> atmosphere ~~Zhu et al. prepared a reduced g-C<sub>3</sub>N<sub>4</sub> material by a thermal treatment with NaBH<sub>4</sub> in N<sub>2</sub> atmosphere~~ [19]. The reduction treatment created nitrogen vacancies followed by a formation of functional group C≡N (Fig. 2), which endowed g-C<sub>3</sub>N<sub>4</sub> with a feature of visible light-driven water oxidation capacity. In addition, the reduction treatment facilitated the spatial separation of photo-excited electron and hole, and enhanced the charge transfer. Therefore, an optimal reduced g-C<sub>3</sub>N<sub>4</sub> obtained enhanced performance in photocatalytic production of H<sub>2</sub>O<sub>2</sub> (170 μmol/L h<sup>-1</sup>) from pure H<sub>2</sub>O and O<sub>2</sub> at ambient atmosphere in the absence of organic electron donors. A parent g-C<sub>3</sub>N<sub>4</sub> was treated with a dielectric barrier discharge (DBD) plasma, and a PT-g-C<sub>3</sub>N<sub>4</sub> material for photocatalytic production of H<sub>2</sub>O<sub>2</sub> was finally obtained. ~~Lu et al. treated the parent g-C<sub>3</sub>N<sub>4</sub> with a dielectric barrier discharge (DBD) plasma to obtain a PT-g-C<sub>3</sub>N<sub>4</sub> material for photocatalytic production of H<sub>2</sub>O<sub>2</sub>~~ [51] (Fig. 3 a). Compared with bare g-C<sub>3</sub>N<sub>4</sub>, PT-g-C<sub>3</sub>N<sub>4</sub> improved the grain size, the surface and pore properties, as well as the hydrophilic property. Furthermore, PT-g-C<sub>3</sub>N<sub>4</sub> significantly improved the H<sub>2</sub>O<sub>2</sub> yield by 13 times based on pristine g-C<sub>3</sub>N<sub>4</sub> (Fig. 3 b).

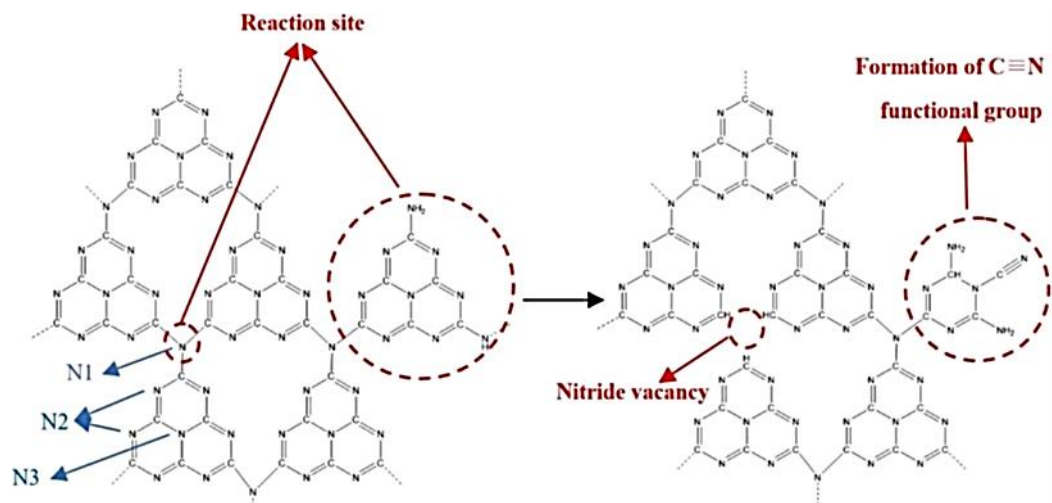


Fig. 2. Probable reaction of g-C<sub>3</sub>N<sub>4</sub> treated with NaBH<sub>4</sub> [19]. [copyright 2018 Elsevier](#).

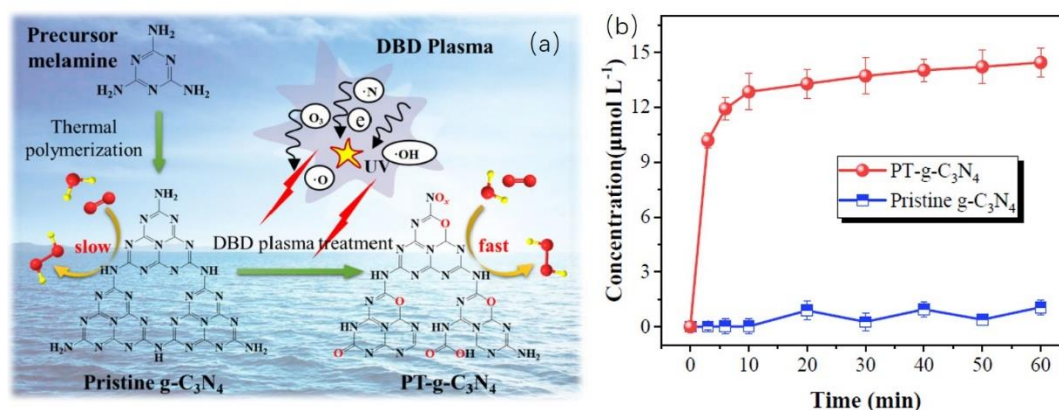


Fig. 3. Mechanism illustration of DBD plasma introducing oxygen-containing functional groups on the surface of  $g\text{-C}_3\text{N}_4$  (a) [51], [copyright 2020 Elsevier](#); photocatalytic activity of pristine  $g\text{-C}_3\text{N}_4$  and PT- $g\text{-C}_3\text{N}_4$  for photocatalytic production of  $\text{H}_2\text{O}_2$  (b) [51], [copyright 2020 Elsevier](#).

## 2.2. Modified $g\text{-C}_3\text{N}_4$ photocatalysts

Introducing the guest molecules or semiconductors to  $g\text{-C}_3\text{N}_4$  host [is effective and frequently used is an effective option](#) to promote the charge separation and the selectivity of the two-electron reduction of  $\text{O}_2$  to  $\text{H}_2\text{O}_2$ . Moreover, the bandgap of  $g\text{-C}_3\text{N}_4$  is easily modulated by doping, hybridization or surface decoration, [resulting in which can promote the](#) effective utilization of visible light [22]. The introduced species mainly include hetero-elements, nanoparticles, semiconductors, organic compounds, polymers [et al.](#) [The modification strategies, photocatalytic performances and properties of the reported  \$g\text{-C}\_3\text{N}\_4\$  based materials for photocatalytic  \$\text{H}\_2\text{O}\_2\$  production are collected in Table 1.](#)

### 2.2.1. Elements doping

Incorporation of earth-abundant heteroelements (K, P or O) can efficiently improve the crystal structure and the band gap of  $g\text{-C}_3\text{N}_4$  to enhanced its photocatalytic performance. [An in situ incorporation of both potassium and phosphate species into the polymeric  \$\text{C}\_3\text{N}\_4\$  framework](#)

~~was reported. Choi's group reported an in situ incorporation of both potassium and phosphate species into the polymeric  $C_3N_4$  framework~~ [52]. The incorporated K, P and O species introduced the negative surface charge, facilitated the interfacial electron transfer to dioxygen, and inhibited the decomposition of in situ generated  $H_2O_2$ . Therefore, the modified  $C_3N_4$  enhanced the apparent quantum yields of  $H_2O_2$  by about 25 and 17 times under monochromatic irradiation of 420 and 320 nm, respectively (Fig. 4 a). The high selectivity toward  $H_2O_2$  over  $H_2$  are attributed to the enhanced light absorption, the increased lifetime of the transient species, the effective interfacial charge transfer to dioxygen, and the inhibited decomposition of in situ generated  $H_2O_2$  (Fig. 4 b). Later, the same group incorporated the potassium hexafluorophosphate into the  $C_3N_4$  structure to obtain a composite photocatalyst (KPF\_CN) [28]. Compared with  $C_3N_4$ , the introduction of  $KPF_6$  could increase the absorption of visible light, the charge carrier density and the selective two-electron transfer to  $O_2$ , and inhibit the photodecomposition of  $H_2O_2$ . The catalyst greatly enhanced the apparent quantum yield of  $H_2O_2$  (26.1 times higher than that of bare  $C_3N_4$ ) in visible light region (Fig. 4 c) (Fig. 4 b). The high selectivity for  $O_2$  reduction in KPF\_CN attributes to the optimized interactions of  $O_2$  molecules and protons with  $K^+$  and  $PF_6^-$  sites, respectively. A series of potassium and phosphorus doped g- $C_3N_4$  catalysts for  $H_2O_2$  photoproduction was synthesized and reported (Fig. 4 d) ~~Tian et al. synthesized a series of potassium and phosphorus doped g- $C_3N_4$  catalysts for  $H_2O_2$  photoproduction~~ [53]. The optimal catalyst achieved 5 mM of  $H_2O_2$  for 10 h, which were 5 folds of that over pure g- $C_3N_4$ . Xue et al. prepared a  $Co_xNi_yP$  cluster incorporated P-doped g- $C_3N_4$  ( $Co_xNi_yP$ -PCN) photocatalyst by a two-step phosphating method [54] (Fig. 5 a-c). It was found that P as a substitution of C in g- $C_3N_4$  introduced a positive charge center ( $P^+$ ) forming a

unique bridging effect. The bridging effect with the extended light absorption by P doping and optimized surface redox potential by cocatalyst integration stimulated efficient vectorial charge transfer between PCN and CoNiP and subsequent surface mass exchange (Fig. 5 d). As a result, the two-electron reaction pathway for H<sub>2</sub>O<sub>2</sub> photogeneration was facilitated.

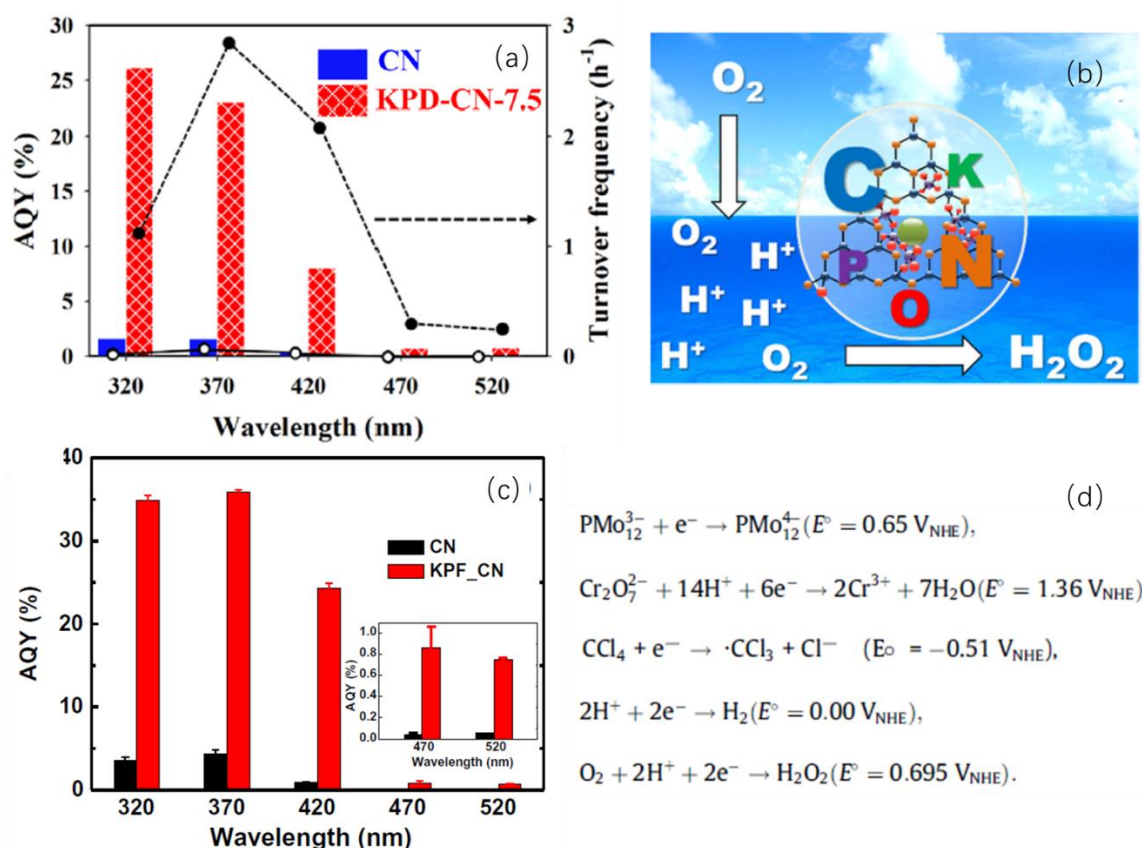


Fig. 4. Apparent quantum yield of H<sub>2</sub>O<sub>2</sub> photoproduction over KPD-CN (a) and the O<sub>2</sub> activation pathway (b) [52], copyright 2017 American Chemical Society; apparent quantum yield of H<sub>2</sub>O<sub>2</sub> photoproduction over KPF\_CN (c) and the O<sub>2</sub> activation pathway (d) [28].

copyright 2018 Elsevier. Apparent quantum yield of H<sub>2</sub>O<sub>2</sub> photoproduction over bare C<sub>3</sub>N<sub>4</sub> and KPD-CN (a) [52], and over bare C<sub>3</sub>N<sub>4</sub> and KPF-CN (b) [28].

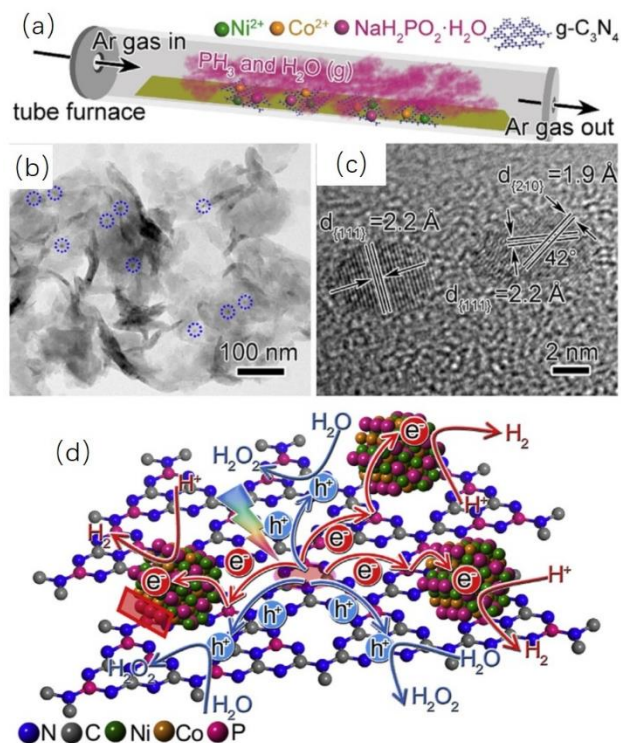


Fig. 5. Schematic illustration for preparation of CoNiP-PCN (a) [54], copyright 2019 Elsevier; TEM (b) and HRTEM (c) images of CoNiP-PCN [54], copyright 2019 Elsevier; proposed mechanism of H<sub>2</sub>O<sub>2</sub> photoproduction over CoNiP-PCN (d) [54], copyright 2019 Elsevier.

In addition, Hu's group prepared a hollow Cu doped g-C<sub>3</sub>N<sub>4</sub> microspheres, in which Cu species was inserted at the interstitial position through the coordinative Cu(I)-N bonds [24]. With a self-established system (Fig. 6 a) for H<sub>2</sub>O<sub>2</sub> photoproduction, the Cu doped g-C<sub>3</sub>N<sub>4</sub> displayed higher H<sub>2</sub>O<sub>2</sub> productivity (4.8 mM) and better structural stability than neat g-C<sub>3</sub>N<sub>4</sub>. With the aid of DFT simulation (Fig. 6 b, c), they concluded that the Cu(I)-N active sites could activate molecular O<sub>2</sub>, and built an "electron transfer bridge" to the adsorbed O<sub>2</sub> molecules.

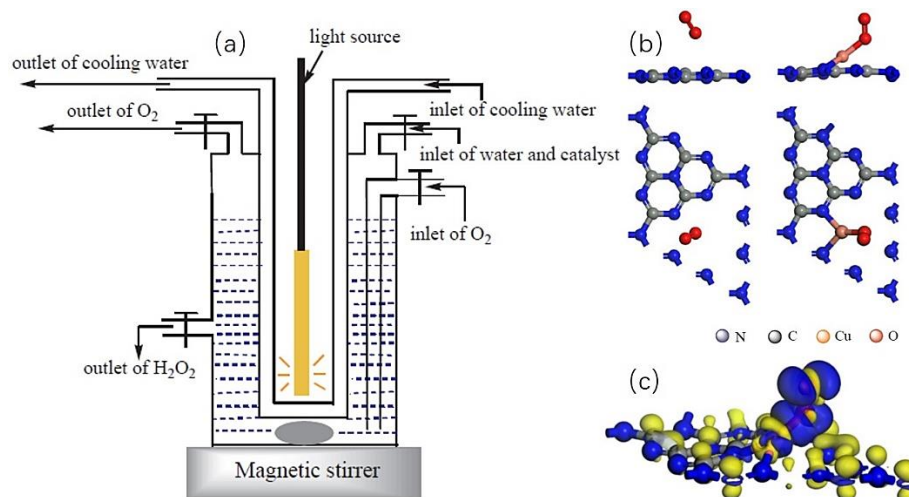


Fig. 6. Schematic diagram of photocatalytic  $\text{H}_2\text{O}_2$  production (a) [24], [copyright 2018 Elsevier](#); Optimal  $\text{O}_2$  adsorption models on  $\text{g-C}_3\text{N}_4$  (left) and Cu doped  $\text{g-C}_3\text{N}_4$  (right) (b) [24], [copyright 2018 Elsevier](#); charge density difference of  $\text{O}_2$  molecule adsorbed on a  $\text{Cu}^+$  doping site (The yellow and blue isosurfaces represent charge accumulation and depletion in the space, respectively) (c) [24], [copyright 2018 Elsevier](#).

### 2.2.2. Surface decoration

Surface modification with functional species or supporting nanoparticles on the parent photocatalyst is an efficient approach to improve the photocatalytic activity by promoting the charge separation and selectively catalyzing relevant reactions. The enhancement effect of Au nanoparticles for  $\text{H}_2\text{O}_2$  generation has been demonstrated over the  $\text{TiO}_2$  photocatalysts [55]. Thereby, Zuo et al. carried out photocatalytic production of  $\text{H}_2\text{O}_2$  over  $\text{g-C}_3\text{N}_4$  supporting Au nanoparticles [56]. Au nanoparticles showed inert nature for the decomposition of  $\text{H}_2\text{O}_2$ , and thus increased the  $\text{H}_2\text{O}_2$  yield. [A boron nitride quantum dots modified ultrathin porous  \$\text{g-C}\_3\text{N}\_4\$  \(BNQDs/UPCN, BU\) composite was constructed via two steps](#) [Yang et al. constructed a boron nitride quantum dots modified ultrathin porous  \$\text{g-C}\_3\text{N}\_4\$  \(BNQDs/UPCN, BU\) composite](#) [57] (Fig. 7 a, b). The superoxide radical ( $\bullet\text{O}_2^-$ ) generation rate over the composite was estimated to



be 2.3 times higher than that over bulky  $g\text{-C}_3\text{N}_4$  (Fig. 7 c), owing to that the composite simultaneously promoted the dissociation of excitons and accelerate the transfer of charges (Fig. 7 d).

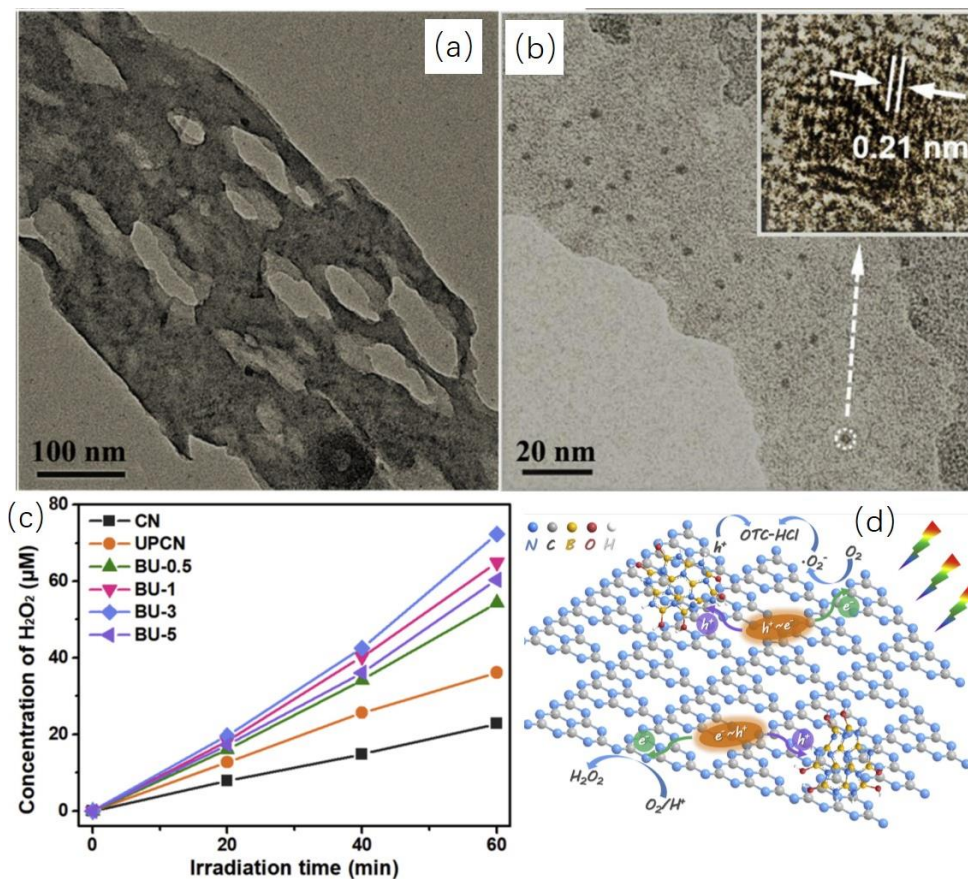


Fig. 7. TEM and HRTEM images of BNQDs/UPCN (a, b) [57], [copyright 2019 Elsevier](#);

$\text{H}_2\text{O}_2$  photoproduction over different BNQDs/UPCN samples (c) [57], [copyright 2019](#)

[Elsevier](#); proposed photocatalytic mechanism in BNQDs/UPCN heterostructure (d) [57],

[copyright 2019 Elsevier](#).

Polyoxometalates (POMs) are classified as metal-oxygen cluster compounds, which can act as electron reservoirs and exhibit extensive ranges of structures and stable redox states [58]. In particular, POMs contain several empty d orbitals that allow them to accept electrons without causing a structural change. These compounds also have nucleophilic oxygen-enriched surfaces



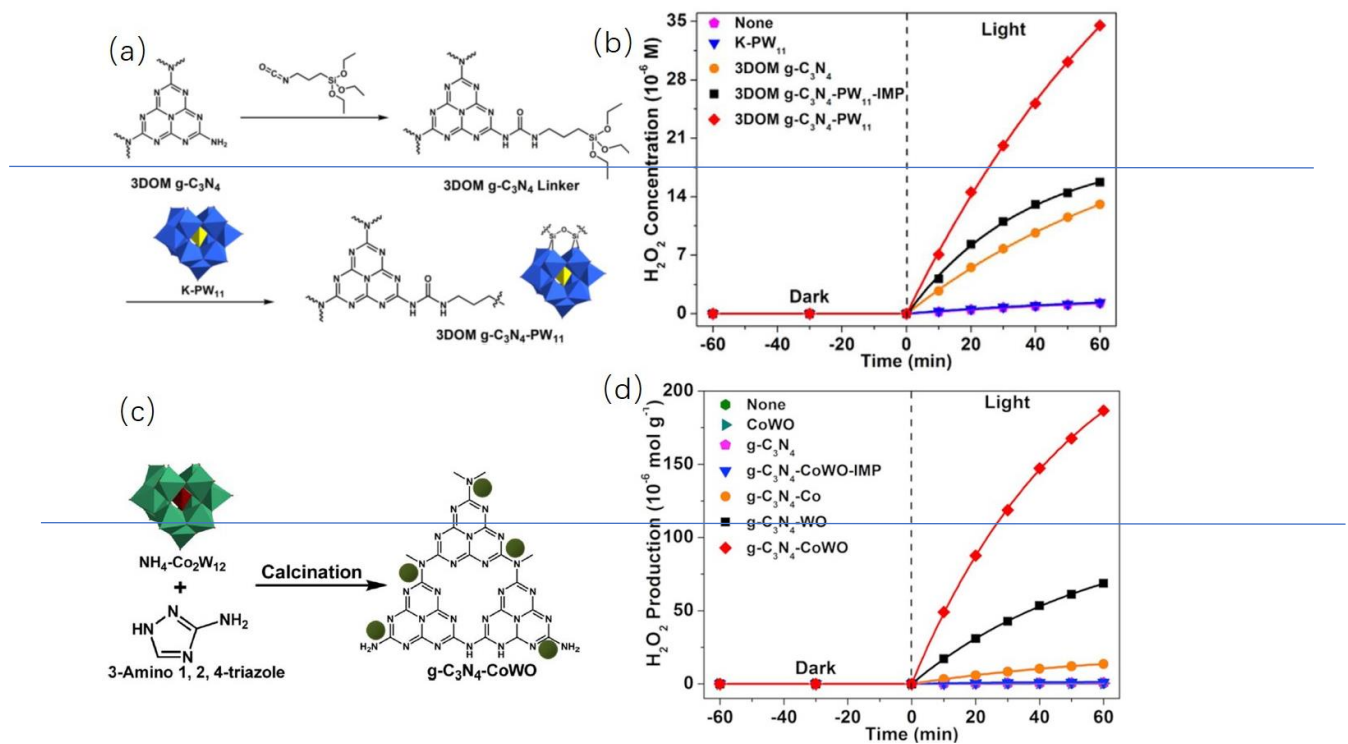


Fig. 8. Photocatalytic  $\text{H}_2\text{O}_2$  formation pathway over  $\text{g-C}_3\text{N}_4$ - $\text{PW}_{11}$  catalyst (a) and its  $\text{H}_2\text{O}_2$  productivity (b) [23], copyright 2017 Elsevier; photocatalytic  $\text{H}_2\text{O}_2$  formation pathway over  $\text{g-C}_3\text{N}_4$ -CoWO (c) and its  $\text{H}_2\text{O}_2$  productivity (d) [60], copyright 2019 Elsevier.

Fig. 8. Preparation process of 3DOM  $\text{g-C}_3\text{N}_4$ - $\text{PW}_{11}$  (a) [23]; photocatalytic  $\text{H}_2\text{O}_2$  formation over different  $\text{g-C}_3\text{N}_4$ - $\text{PW}_{11}$  catalysts (b) [23]; preparation process of  $\text{g-C}_3\text{N}_4$ -CoWO (c) [60]; photocatalytic  $\text{H}_2\text{O}_2$  formation over different  $\text{g-C}_3\text{N}_4$ -CoWO catalysts (d) [60].

Organic compounds and organisms are also practiced in photocatalytic  $\text{H}_2\text{O}_2$  production to become good cocatalysts of  $\text{g-C}_3\text{N}_4$ . An all-solid-state Z-scheme heterojunction (PI-NCN) was constructed by assembling perylene imides (PI) on  $\text{g-C}_3\text{N}_4$  nanosheets (NCN) via gas soft-template and condensation reaction method Yang et al. constructed an all-solid-state Z-scheme heterojunction (PI-NCN) by assembling perylene imides (PI) on  $\text{g-C}_3\text{N}_4$  nanosheets (NCN) [18].

Electrons in conduction band of PI were transferred into the valence band of  $\text{g-C}_3\text{N}_4$  by photoexcitation, which provided more electrons for the reduction of  $\text{O}_2$  to generate more  $\text{H}_2\text{O}_2$ .

Therefore, PI could change  $\text{H}_2\text{O}_2$  generation from single-channel to two-channel route. Fu et al. were inspired by the behavior of chlorella as a biological  $\text{H}_2\text{O}_2$  generator, and prepared a living chlorella vulgaris and carbon micro particle (needle coke) co-modified g- $\text{C}_3\text{N}_4$  (C-N-g- $\text{C}_3\text{N}_4$ ) photocatalyst [61]. The novel material achieved the simultaneous photocatalytic water splitting and biological  $\text{H}_2\text{O}_2$  generation with  $\text{H}_2\text{O}_2$  productivity of  $0.98 \mu\text{mol h}^{-1}$ .

### 2.2.3. Hybridization

Hybridization is a widely accepted approach to obtain an efficient and stable photocatalyst of heterojunction. A hybrid catalyst of g- $\text{C}_3\text{N}_4$  and carbon nanotubes (g- $\text{C}_3\text{N}_4$ -CNTs) with well-defined and stable structure was prepared through an amidation reaction ~~Zhao et al. prepared a hybrid catalyst of g- $\text{C}_3\text{N}_4$  and carbon nanotubes (g- $\text{C}_3\text{N}_4$ -CNTs) with well defined and stable structure through an amidation reaction~~ [27]. The CNTs covalent combined with g- $\text{C}_3\text{N}_4$  promoted the electrons generation (Fig. 9 a). Therefore, the single-electron reduction of  $\text{O}_2$  to  $\bullet\text{O}_2^-$  and the sequential two-step single-electron  $\text{O}_2$  reduction reaction was promoted successively (Fig. 9 a). The hybrid catalyst obtained  $32.6 \mu\text{mol}\cdot\text{h}^{-1}$  of  $\text{H}_2\text{O}_2$  productivity in the presence of formic acid under visible light. A  $\text{Cu}_2(\text{OH})\text{PO}_4/\text{g-}\text{C}_3\text{N}_4$  composite was prepared via the hydrothermal and co-calcination procedures for photocatalytic  $\text{H}_2\text{O}_2$  production ~~Wang et al. prepared a  $\text{Cu}_2(\text{OH})\text{PO}_4/\text{g-}\text{C}_3\text{N}_4$  composite for photocatalytic  $\text{H}_2\text{O}_2$  production~~ [62].  $\text{Cu}_2(\text{OH})\text{PO}_4$  could adsorb  $\text{O}_2$  molecules, and formed photogenerated electrons to recombine the holes in g- $\text{C}_3\text{N}_4$  through a Z-scheme mechanism. The heterojunction catalyst with 20 wt.% of  $\text{Cu}_2(\text{OH})\text{PO}_4$  obtained 7.2 mM of  $\text{H}_2\text{O}_2$ , which was over 13 times higher than that of pure g- $\text{C}_3\text{N}_4$ . An interfacial Schottky junction composed of  $\text{Ti}_3\text{C}_2$  nanosheets and porous g- $\text{C}_3\text{N}_4$  nanosheets (TC/pCN) was fabricated via an electrostatic self-assembly route ~~Yang et al.~~

fabricated an interfacial Schottky junction composed of  $\text{Ti}_3\text{C}_2$  nanosheets and porous  $\text{g-C}_3\text{N}_4$  nanosheets (TC/pCN) via an electrostatic self-assembly route [63]. The formation of Schottky junction and subsequent built-in electric field at their interface accelerated the spatial charge separation and restrain the charge recombination (Fig. 9 b). TC/pCN exhibited a high  $\text{H}_2\text{O}_2$  yield ( $2.20 \mu\text{mol L}^{-1} \text{min}^{-1}$ ) under visible light irradiation ( $\lambda > 420 \text{ nm}$ ), which is about 2.1 times higher than that of bare  $\text{g-C}_3\text{N}_4$ .

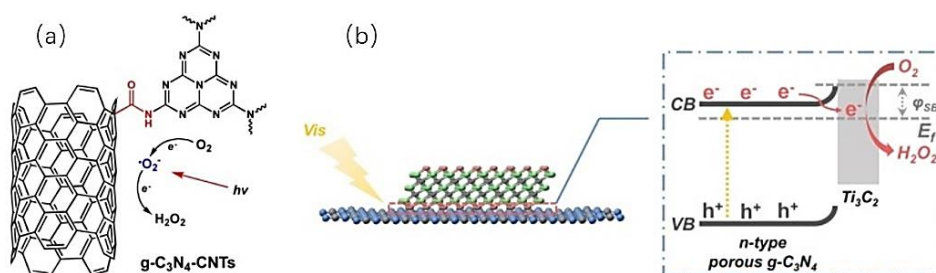


Fig. 9. Schematic diagram of photocatalytic  $\text{H}_2\text{O}_2$  production over  $\text{g-C}_3\text{N}_4$ -CNTs (a) [27],

copyright 2018 Elsevier, and TC/pCN (b) [63], copyright 2019 Elsevier.

The  $\text{g-C}_3\text{N}_4$  based materials have unique structure of tri-s-triazine moieties which can promote selective two-electron transfer to  $\text{O}_2$  via sequential formation of a superoxo radical and 1,4-endoperoxide species to facilitates  $\text{H}_2\text{O}_2$  generation under visible light irradiation [64]. The yield and selectivity of  $\text{H}_2\text{O}_2$  can be enhanced via the improvements in the surface, oxygen affinity, charge separation, proton-coupled electron transfer, and  $\text{H}_2\text{O}_2$  decomposition retardation of  $\text{g-C}_3\text{N}_4$  catalysts. Therefore, the strategies of morphology control, hetero-elements doping, surface modification and hybridization for  $\text{g-C}_3\text{N}_4$  are expected to be further updated and reported. Scaling up of  $\text{H}_2\text{O}_2$  production can be achieved by the development of  $\text{g-C}_3\text{N}_4$  materials and their system engineering.

Table 1 Summary of the modification strategies, photocatalytic performances and properties of the reported g-C<sub>3</sub>N<sub>4</sub> based materials for photocatalytic H<sub>2</sub>O<sub>2</sub> production.

<u>Photocatalyst</u>	<u>Modification strategy</u>	<u>Reaction system</u>	<u>H<sub>2</sub>O<sub>2</sub> productivity</u>	<u>Reference</u>
<u>g-C<sub>3</sub>N<sub>4</sub></u>	<u>Pristine</u>	<u>Visible light; 5 mL</u> <u>Alcohol/water; O<sub>2</sub></u>	<u>30 μmol (24h)</u>	[21]
<u>g-C<sub>3</sub>N<sub>4</sub>/PDI</u>	<u>Mixture heating</u>	<u>Visible light; 50 mL</u> <u>Water; O<sub>2</sub></u>	<u>50.6 μM (48h)</u>	[48]
<u>Mesoporous g-C<sub>3</sub>N<sub>4</sub></u>	<u>Silica-templated</u> <u>thermal</u> <u>polymerization</u>	<u>Visible light; 5 mL</u> <u>EtOH/water; O<sub>2</sub></u>	<u>90 μmol (24h)</u>	[26]
<u>C<sub>3</sub>N<sub>4</sub> aerogel</u>	<u>Self-assembly</u>	<u>Visible light; 30 mL</u> <u>water; O<sub>2</sub></u>	<u>36 μmol (25 h)</u>	[49]
<u>g-C<sub>3</sub>N<sub>4</sub></u>	<u>Carbon vacancy-</u> <u>based strategy</u>	<u>Visible light; 100 mL</u> <u>water; O<sub>2</sub></u>	<u>~ 90 μM (1 h)</u>	[50]
<u>Reduced g-C<sub>3</sub>N<sub>4</sub></u>	<u>Thermal treatment</u> <u>with NaBH<sub>4</sub></u>	<u>Visible light; 100 mL</u> <u>water; O<sub>2</sub></u>	<u>170 μM (1 h)</u>	[19]
<u>g-C<sub>3</sub>N<sub>4</sub></u>	<u>dielectric barrier</u> <u>discharge plasma</u> <u>modification</u>	<u>Visible light; 60 mL</u> <u>water</u>	<u>27 μM (1 h)</u>	[51]
<u>K, P, O-C<sub>3</sub>N<sub>4</sub></u>	<u>Calcination with</u> <u>K<sub>2</sub>HPO<sub>4</sub></u>	<u>Visible light; 40 mL</u> <u>EtOH/water; O<sub>2</sub></u>	<u>1.7 mM (7 h)</u>	[52]
<u>KPF<sub>6</sub>-C<sub>3</sub>N<sub>4</sub></u>	<u>Thermal</u>	<u>Visible light;</u>	<u>1.5 mM (5 h)</u>	[28]

---

	<u>polymerization</u>	<u>EtOH/water; O<sub>2</sub></u>		
<u>Hollow Cu-doped g-C<sub>3</sub>N<sub>4</sub></u>	<u>Template method</u>	<u>Visible light; 200 mL water; 80 mL/min of O<sub>2</sub> bubbling</u>	<u>4.5 mM (4 h)</u>	[24]
<u>Au/C<sub>3</sub>N<sub>4</sub></u>	<u>KBH<sub>4</sub> reduction</u>	<u>Visible light; 100 mL EtOH/water (pH = 8.5); O<sub>2</sub></u>	<u>2 mM (30 h)</u>	[56]
<u>BNQDs/UPCN</u>	<u>Two steps</u>	<u>Visible light; 50 mL isopropanol/water; O<sub>2</sub></u>	<u>74 μM (1 h)</u>	[57]
<u>3DOM g-C<sub>3</sub>N<sub>4</sub>-PW<sub>11</sub></u>	<u>Covalent combining and organic linker strategy</u>	<u>Visible light; 100 mL water; O<sub>2</sub></u>	<u>14.4 μmol (6 h)</u>	[23]
<u>g-C<sub>3</sub>N<sub>4</sub>-CoWO<sub>4</sub></u>	<u>Precursor co-calcination</u>	<u>Visible light; 100 mL water; O<sub>2</sub></u>	<u>9.7 μmol (1 h)</u>	[60]
<u>PI-NCN</u>	<u>Gas soft-template and condensation reaction method</u>	<u>Visible light; 50 mL water</u>	<u>124 μmol (2h)</u>	[18]
<u>C-N-g-C<sub>3</sub>N<sub>4</sub></u>	<u>Living Chlorella vulgaris and carbon micro particle modification</u>	<u>Visible light; 15 mL water; O<sub>2</sub></u>	<u>12.1 μmol (12 h)</u>	[61]
<u>g-C<sub>3</sub>N<sub>4</sub>-CNTs</u>	<u>Amidation reaction</u>	<u>Visible light; 100 ml of</u>	<u>53.8 μmol (4 h)</u>	[27]

---

---

		<u>formic acid/water; O<sub>2</sub></u>		
<u>Cu<sub>2</sub>(OH)PO<sub>4</sub>/g-</u>	<u>Hydrothermal and co-</u>	<u>Simulated solar light</u>	<u>8.9 mM (18 h)</u>	[62]
<u>C<sub>3</sub>N<sub>4</sub></u>	<u>calcination</u>	<u>source; 200 mL water;</u>		
		<u>80 mL/min of O<sub>2</sub></u>		
		<u>bubbling</u>		
<u>Ti<sub>3</sub>C<sub>2</sub>/porous g-</u>	<u>Electrostatic self-</u>	<u>Visible light; 50 mL</u>	<u>131.71 μmol (1 h)</u>	[63]
<u>C<sub>3</sub>N<sub>4</sub></u>	<u>assembly route</u>	<u>isopropanol/water; O<sub>2</sub></u>		

---

### 3. Photocatalytic production of H<sub>2</sub>O<sub>2</sub> over TiO<sub>2</sub> based materials

TiO<sub>2</sub> based photocatalysts are one of the preferred families for H<sub>2</sub>O<sub>2</sub> production due to their merits of chemical stability, low cost and practical application. Before H<sub>2</sub>O<sub>2</sub> production over TiO<sub>2</sub> becomes commercial, it should overcome two difficulties including the side reaction of one electron oxygen reduction, and the serious decomposition of H<sub>2</sub>O<sub>2</sub> catalyzed by the intermediate of ≡Ti-OOH. The improved strategies and the categorization for TiO<sub>2</sub> are similar to that for the abovementioned g-C<sub>3</sub>N<sub>4</sub> catalysts. [The modification strategies, photocatalytic performances and properties of the reported TiO<sub>2</sub> based materials for photocatalytic H<sub>2</sub>O<sub>2</sub> production are collected in Table 2.](#)

Single TiO<sub>2</sub> catalyst has obtained the satisfied yield of H<sub>2</sub>O<sub>2</sub>. Cai et al. earlier researched photocatalytic production of H<sub>2</sub>O<sub>2</sub> over TiO<sub>2</sub> [65]. In their work, the effect of copper ions on the formation of H<sub>2</sub>O<sub>2</sub> was investigated. In an O<sub>2</sub> purged solution, H<sub>2</sub>O<sub>2</sub> productivity was increased to 20 times in the presence of moderate amount of copper ions. Shiraishi's group tried to use benzylic alcohols as hydrogen sources for light driven H<sub>2</sub>O<sub>2</sub> production with TiO<sub>2</sub> photocatalyst [31]. They revealed that the enhanced H<sub>2</sub>O<sub>2</sub> formation was due to the efficient



formation of side-on coordinated per oxo species on the photoactivated TiO<sub>2</sub> surface, via the reaction of benzylic alcohol and O<sub>2</sub>. The peroxy species was readily transformed to H<sub>2</sub>O<sub>2</sub>, thus facilitating highly efficient H<sub>2</sub>O<sub>2</sub> production. The band gap photoexcitation of TiO<sub>2</sub> also promoted the selectivity of H<sub>2</sub>O<sub>2</sub>. In another earlier report, the effect of Zn(II) on the formation of H<sub>2</sub>O<sub>2</sub> over TiO<sub>2</sub> was investigated ~~Maurino et al. investigated the effect of Zn(II) on the formation of H<sub>2</sub>O<sub>2</sub> catalyzed by TiO<sub>2</sub>~~ [66]. In this work, ~~they~~ the researchers provided the mechanism and kinetic of interfacial electron transfer by blocking surface trapping sites for photogenerated carriers ( $\equiv\text{Ti-OH}$ ).

There are a number of works on the surface modification strategies for TiO<sub>2</sub> to enhance its H<sub>2</sub>O<sub>2</sub> photoproduction. For examples, a Pt/TiO<sub>2</sub> photocatalytic system simultaneously achieved the H<sub>2</sub> and the H<sub>2</sub>O<sub>2</sub> production ~~Wang et al. introduced a Pt/TiO<sub>2</sub> photocatalytic system to achieve simultaneous H<sub>2</sub> and H<sub>2</sub>O<sub>2</sub> production~~ [67]. H<sub>2</sub>O<sub>2</sub> productivity reached 5096  $\mu\text{mol g}^{-1} \text{h}^{-1}$ , which was attributed to the more favorable two-electron oxidation of water to H<sub>2</sub>O<sub>2</sub> than the four-electron oxidation of water to O<sub>2</sub>. A negative charged Pd nanoparticles loaded on TiO<sub>2</sub> photocatalyst was prepared by coordinating Pd with surface-anchored organic ligands ~~Chu et al. developed a negative charged Pd nanoparticles loaded on TiO<sub>2</sub> photocatalyst by coordinating Pd with surface-anchored organic ligands~~ [68]. ~~They confirmed that the~~ The negative charge on the Pd were induced by the electron donation from amine groups of the ligands. For photocatalytic production of H<sub>2</sub>O<sub>2</sub>, a mechanism was proposed that the electronic tuning of Pd nanoparticles enhanced the charge separation on TiO<sub>2</sub>, which improved the selectivity of O<sub>2</sub> reduction to produce H<sub>2</sub>O<sub>2</sub>. The improved selectivity for H<sub>2</sub>O<sub>2</sub> production was over the side reactions such as O<sub>2</sub> reduction to water (Pathway 1, Fig. 10). O<sub>2</sub> reduction occurred on the Pd

surface given the high affinity of O<sub>2</sub> to Pd, generating surface-bound superoxide by the first electron transfer. The selectivity for H<sub>2</sub>O<sub>2</sub> production is determined by the subsequent competing coordination reactions:  $\mu$ -peroxo coordination followed by homolytic O–O bond cleavage (Pathway 1, with water as final product, Fig. 10) vs protonation (Pathway 2, with H<sub>2</sub>O<sub>2</sub> as final product, Fig. 10). ~~(Fig. 10). A porous TiO<sub>2</sub> films supporting Au nano island was exploited as the photocatalyst of light driven H<sub>2</sub>O<sub>2</sub> production~~ Kim et al. reported a porous TiO<sub>2</sub> films supporting Au nano island as photocatalyst of light driven H<sub>2</sub>O<sub>2</sub> production [69] (Fig. 11 a). H<sub>2</sub>O<sub>2</sub> concentration over the catalyst achieved the mM scale within 5 min, which was 80 folds based on pure TiO<sub>2</sub> (Fig. 11 b). The combination of small Au, TiO<sub>2</sub>, and large Au species reduced the potential barriers, and thus reduced the recombination of electron-hole pairs. A CuO incorporated TiO<sub>2</sub> catalyst was earlier prepared for light driven H<sub>2</sub>O<sub>2</sub> production Bandara et al. prepared a CuO incorporated TiO<sub>2</sub> catalyst for light driven H<sub>2</sub>O<sub>2</sub> production [33]. Modification of CuO promoted the charge separation and provided active sites for water reduction. In detail, photoexcited electrons in CB of both TiO<sub>2</sub> and CuO, and the accumulation of excess electrons in CuO caused a negative shift in the Fermi level, which gained the required overvoltage necessary for efficient water reduction reaction. Zheng et al. modified TiO<sub>2</sub> with S and N co-doped graphene quantum dots (SNGQD/TiO<sub>2</sub>) for photocatalytic production of H<sub>2</sub>O<sub>2</sub> [70]. SNGQD induced the extended visible light absorption and enhanced electron migration. The catalyst exhibited 3.2 times of H<sub>2</sub>O<sub>2</sub> yield (451  $\mu\text{mol L}^{-1}$ ) as that of bare TiO<sub>2</sub> under simulated sunlight irradiation. The increased H<sub>2</sub>O<sub>2</sub> was attributed to the boosted two-electron reduction of oxygen, as well as the suppressed decomposition of H<sub>2</sub>O<sub>2</sub>. Koutecky-Levich plots and DFT calculations demonstrated that the kinetic rate of ORR was accelerated by GQDs with the

facilitated charge transfer, and the two-electron ORR pathway rationalized the high selectivity for  $\text{H}_2\text{O}_2$  formation. In another work of Zheng [71], a novel nafion coatings on S,N-codoped graphene-quantum-dots-modified  $\text{TiO}_2$  (NF-SNG/ $\text{TiO}_2$ ) catalyst also presented the enhanced photocatalytic performance of  $\text{H}_2\text{O}_2$  photoproduction.

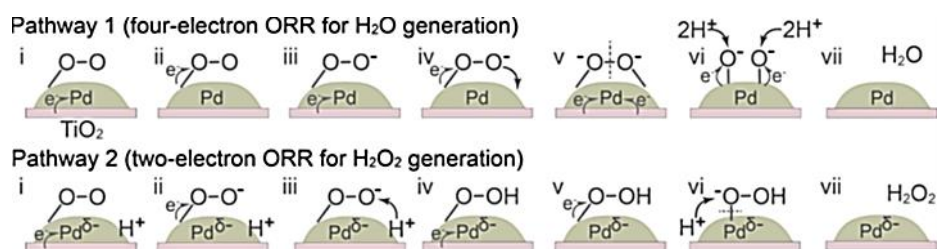


Fig. 10. Mechanisms of oxygen reduction on the surface of Pd nanoparticles [68]. copyright

2019 American Chemical Society.

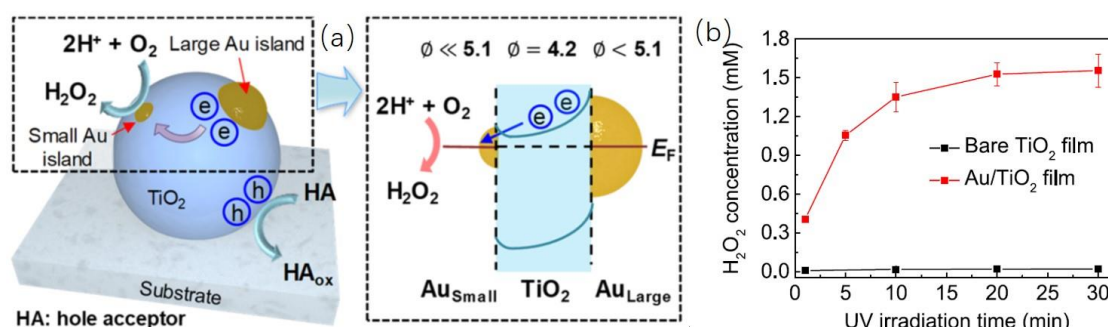


Fig. 11. Schematic diagram of photocatalytic  $\text{H}_2\text{O}_2$  production over Au/ $\text{TiO}_2$  films (a) [69].

copyright 2019 American Chemical Society; time-dependent  $\text{H}_2\text{O}_2$  production over bare  $\text{TiO}_2$  and Au/ $\text{TiO}_2$  films (b) [69]. copyright 2019 American Chemical Society.

Hybridization of carbon materials with  $\text{TiO}_2$  based photocatalysts has also been attempted in photocatalytic  $\text{H}_2\text{O}_2$  production. For examples, a hybrid material of proton-form titania nanotube with carbon dot (HTNT-CD) was exploited for  $\text{H}_2\text{O}_2$  photoproduction. Ma et al. reported a hybrid catalyst of proton-form titania nanotube with carbon dot (HTNT-CD) for  $\text{H}_2\text{O}_2$  production [72]. It was demonstrated that the protons of HTNT-CD were crucial for acceleration of the half reaction of molecular  $\text{O}_2$  reduction to form  $\text{H}_2\text{O}_2$ , and hindering the  $\text{H}_2\text{O}_2$

decomposition. The HTNT-CD hybrid obtained 5.2% of the solar-to-H<sub>2</sub>O<sub>2</sub> apparent energy conversion efficiency, which was about 5 times of that over P25 catalyst. In addition, a reduced graphene oxide and TiO<sub>2</sub> (rGO/TiO<sub>2</sub>) hybrid system further increased H<sub>2</sub>O<sub>2</sub> yield to a mmol scale via the adsorption of phosphate on TiO<sub>2</sub> ~~Moon et al. established a reduced graphene oxide and TiO<sub>2</sub> (rGO/TiO<sub>2</sub>) hybrid system for photocatalytic production of H<sub>2</sub>O<sub>2</sub>, and further increased H<sub>2</sub>O<sub>2</sub> yield to a mmol scale via the adsorption of phosphate on TiO<sub>2</sub> [32].~~

TiO<sub>2</sub> based materials have the potential to become mature photocatalysts for visible light-driven H<sub>2</sub>O<sub>2</sub> production due to the merits of chemical stability and low cost. However, there are two challenges restricting this application of TiO<sub>2</sub>: 1) the dominated inefficient single-electron O<sub>2</sub> reduction; 2) the simultaneous decomposition of H<sub>2</sub>O<sub>2</sub> by forming peroxide complexes (≡Ti-OOH) [71]. Therefore, more studies are being concentrated on doping, hybridization or surface decoration for TiO<sub>2</sub> to achieve highly selective two-electron reduction of O<sub>2</sub> and inhibition of photodecomposition of H<sub>2</sub>O<sub>2</sub>.

Table 2 Summary of the modification strategies, photocatalytic performances and properties of the reported TiO<sub>2</sub> based materials for photocatalytic H<sub>2</sub>O<sub>2</sub> production.

<u>Photocatalyst</u>	<u>Modification strategy</u>	<u>Reaction system</u>	<u>H<sub>2</sub>O<sub>2</sub> productivity</u>	<u>Reference</u>
<u>TiO<sub>2</sub></u>	<u>Pristine</u>	<u>UV irradiation; 3 mL water, Cu<sup>2+</sup>; O<sub>2</sub></u>	<u>8 μM (5 min)</u>	<u>[65]</u>
<u>TiO<sub>2</sub></u>	<u>Pristine</u>	<u>Visible light; 5 mL benzyl</u>	<u>40 mM (12 h)</u>	<u>[31]</u>

---

		<u>alcohol/water; O<sub>2</sub></u>		
<u>Pt/TiO<sub>2</sub></u>	<u>In-situ photo-</u>	<u>Visible light; 20</u>	<u>5.1 mmol (1 h)</u>	[67]
	<u>deposition method</u>	<u>mL water</u>		
<u>Pd/TiO<sub>2</sub></u>	<u>Coordination with</u>	<u>Visible light;</u>	<u>150 μM (1 h)</u>	[68]
	<u>surface-anchored</u>	<u>phosphate buffer</u>		
	<u>organic ligands</u>			
<u>Au/porous TiO<sub>2</sub></u>	<u>Thermal</u>	<u>365 nm UV lamp</u>	<u>1.5 mM (0.5 h)</u>	[69]
<u>film</u>	<u>evaporator</u>	<u>irradiation;</u>		
		<u>Ethanol/Citrate</u>		
		<u>buffer, pH 3.8</u>		
<u>SN-GQD/TiO<sub>2</sub></u>	<u>Hydrothermal and</u>	<u>Visible light; 50</u>	<u>451 μM (1 h)</u>	[70]
	<u>impregnation</u>	<u>mL water/2-</u>		
		<u>propanol (pH = 3)</u>		
<u>Nf-SNG/TiO<sub>2</sub></u>	<u>Nafion coating</u>	<u>Visible light; 50</u>	<u>780 μM (2 h)</u>	[71]
		<u>mL water/2-</u>		
		<u>propanol (pH = 3)</u>		
<u>HTNT-CD</u>	<u>Hydrothermal</u>	<u>Visible light; 30</u>	<u>110 μmol (2 h)</u>	[72]
	<u>method</u>	<u>mL water; O<sub>2</sub></u>		
<u>CoPirGO/TiO<sub>2</sub></u>	<u>In-situ formation</u>	<u>Visible light; 40</u>	<u>4.6 mM (3 h)</u>	[32]
	<u>of cobalt</u>	<u>mL water/2-</u>		
	<u>phosphate on</u>	<u>propanol; O<sub>2</sub></u>		
	<u>photocatalyst</u>			

---

#### 4. Photocatalytic production of H<sub>2</sub>O<sub>2</sub> over transition metal complexes

Metal complexes including the metal-organic frameworks (MOFs) are another family for photocatalytic production of H<sub>2</sub>O<sub>2</sub>. [The modification strategies, photocatalytic performances and properties of the reported transition metal complexes for photocatalytic H<sub>2</sub>O<sub>2</sub> production are collected in Table 3.](#)

##### 4.1. Metal-organic frameworks

[Recently, a MIL-125-NH<sub>2</sub> MOFs material for photocatalytic H<sub>2</sub>O<sub>2</sub> production in a benzylalcohol/water two-phase system was exploited and reported](#) ~~Yamashita's group used a MIL-125-NH<sub>2</sub> MOFs material for photocatalytic H<sub>2</sub>O<sub>2</sub> production in a benzylalcohol/water two-phase system~~ [73] (Fig. 12 a). Hydrophobization of MOF enabled the spontaneous separation of the benzaldehyde formed to the benzylalcohol phase and of the H<sub>2</sub>O<sub>2</sub> formed to the aqueous phase (Fig. 12 b). The novel system enhanced the photocatalytic efficiency and adapted various mediums including a solution of low pH for H<sub>2</sub>O<sub>2</sub> production. Meanwhile, the same group modified MIL-125-NH<sub>2</sub> MOFs via alkylation of octadecylphosphonic acid (OPA/MIL-125-NH<sub>2</sub>) as a photocatalyst for H<sub>2</sub>O<sub>2</sub> production [74] (Fig. 12 c). The enhanced photocatalytic performance originated from Ti cluster-alkylated hydrophobic property, and the faster diffusion of reactants and products in the maintained pores of the MOFs.

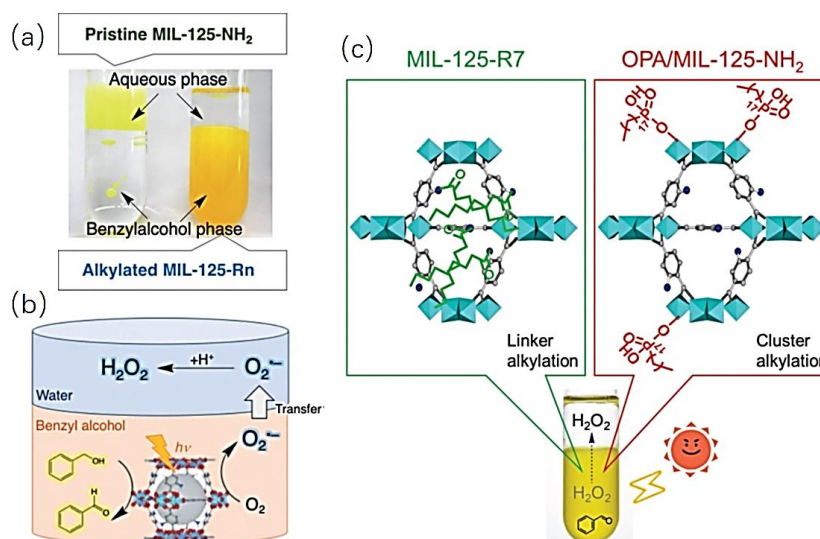


Fig. 12. Photographs of two-phase systems composed of an aqueous phase and a benzylalcohol phase containing MIL-125-NH<sub>2</sub> (left) and MIL-125-Rn (right) (a); photocatalytic H<sub>2</sub>O<sub>2</sub> production utilizing the two-phase system (b) [73], [copyright 2019 Wiley](#); structures of linker-alkylated MIL-125-NH<sub>2</sub>, MIL-125-R7 (top left), cluster-alkylated MIL-125-NH<sub>2</sub>, OPA/MIL-125-NH<sub>2</sub> (top right), and photocatalytic H<sub>2</sub>O<sub>2</sub> production over the MOFs system [74], [copyright 2019 Royal Society of Chemistry](#).

#### 4.2. Novel transition metal complexes

In 2005, Hayes et al. earlier reported Zn(II)-centered complexes acting as photocatalysts for H<sub>2</sub>O<sub>2</sub> production in an ultraviolet irradiated environment [75]. In this work, various ligands of amino-substituted isomers including indazole, pyridine, and phenylenediamine et al. were tested to catalyze the reaction. Among them, Zn-5-aminoindazole obtained the greatest first-day production of 63 mM/day with a 37% quantum yield and *p*-phenylenediamine (PPAM) showed the greatest long-term stability.

After that, most of the reports on applying the transition metal complexes in photocatalytic H<sub>2</sub>O<sub>2</sub> production were from Fukuzumi's group. [For examples, they Yamada et al.](#) reported photocatalytic H<sub>2</sub>O<sub>2</sub> production over a complex catalyst of 2-phenyl-4-(1-naphthyl)quinolinium

ion ( $\text{QuPh}^+-\text{NA}$ ) with oxalate or oxalic acid as electron donor [46, 47].  $\text{QuPh}^+-\text{NA}$  formed the long-lived electron-transfer state upon the photoexcitation with strong oxidation ability. In an oxygen saturated mixed solution of a buffer and acetonitrile, 14% of quantum yield and 93% of  $\text{H}_2\text{O}_2$  yield were obtained. ~~Kato et al. used~~  $[\text{Ru}(\text{Me}_2\text{phen})_3]^{2+}$  ( $\text{Me}_2\text{phen} = 4,7\text{-dimethyl-1,10-phenanthroline}$ ) and  $\text{Ir}(\text{OH})_3$  was used as photocatalysts for water oxidation in an  $\text{O}_2$ -saturated  $\text{H}_2\text{SO}_4$  aqueous solution [43].  $\text{H}_2\text{O}_2$  was produced from the formation of  $[\text{Ru}^{\text{III}}(\text{Me}_2\text{phen})_3]^{3+}$  and  $\cdot\text{O}^{2-}$ , which resulted from the electron transfer from the excited state of  $[\text{Ru}^{\text{II}}(\text{Me}_2\text{phen})_3]^{2+}$  to  $\text{O}_2$ . Photocatalytic activity was further improved by replacing  $\text{Ir}(\text{OH})_3$  nanoparticles by  $[\text{Co}^{\text{III}}(\text{Cp}^*)(\text{bpy})(\text{H}_2\text{O})]^{2+}$  in the presence of  $\text{Sc}(\text{NO}_3)_3$  in water (Fig. 13 a). After that, they Isaka et al. employed nanoparticles composed of earth abundant nickel and iron ( $\text{NiFe}_2\text{O}_4$ ) instead of the Ir complex as a water oxidation catalyst for the photocatalytic production of  $\text{H}_2\text{O}_2$  [44]. During the reaction,  $\text{NiFe}_2\text{O}_4$  nanoparticles were formed from the corresponding as-prepared  $\text{NiFe}_2\text{O}_4$ . The  $\text{H}_2\text{O}_2$  productivity also achieved improvement. They Isaka et al. also used cyano-bridged a polynuclear complexes  $(\text{Fe}_x\text{Co}_{1-x})_3 [\text{Co}(\text{CN})_6]_2$  as effective catalysts for photocatalytic  $\text{H}_2\text{O}_2$  production in an  $\text{O}_2$ -saturated aqueous solution in the presence of  $[\text{Ru}(\text{Me}_2\text{phen})_3]^{2+}$  and  $\text{Sc}(\text{NO}_3)_3$  under visible light irradiation [41]. Cobalt chlorin derivatives ( $\text{Co}^{\text{II}}(\text{Ch}_n)$  ( $n = 1-3$ )) was used ~~Mase et al. used cobalt chlorin derivatives ( $\text{Co}^{\text{II}}(\text{Ch}_n)$  ( $n = 1-3$ ))~~ as catalyst for investigation on the mechanism of photocatalytic  $\text{H}_2\text{O}_2$  production [45]. Nonsubstituted cobalt chlorin complex ( $\text{Co}^{\text{II}}(\text{Ch}_1)$ ) efficiently and selectively catalyzed two-electron reduction of  $\text{O}_2$  by a one-electron reductant (1,1'-dimethylferrocene) to produce  $\text{H}_2\text{O}_2$  in the presence of perchloric acid ( $\text{HClO}_4$ ) in benzonitrile (Fig. 13 b). The change in redox property resulted in the enhancement of the catalytic reactivity, where the observed rate constant



( $k_{\text{obs}}$ ) value of  $\text{Co}^{\text{II}}(\text{Ch}_3)$  was 36-fold larger than that of  $\text{Co}^{\text{II}}(\text{Ch}_1)$  (Fig. 13 b).

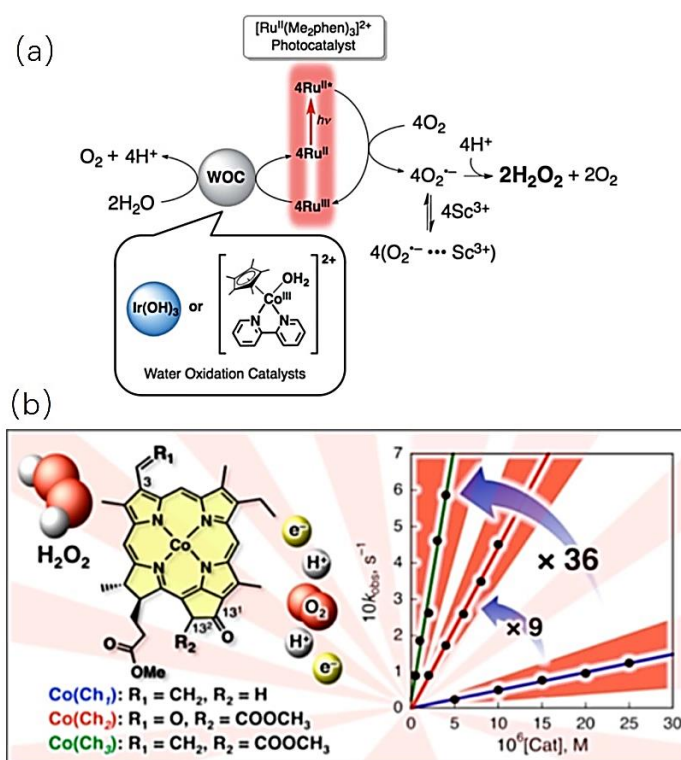


Fig. 13. Schematic diagram of photocatalytic  $\text{H}_2\text{O}_2$  production over  $[\text{Ru}^{\text{II}}(\text{Me}_2\text{phen})_3]^{2+}$ - $\text{Ir}(\text{OH})_3\text{-Sc}^{3+}$  system (a) [43], [copyright 2013 Royal Society of Chemistry](#), and  $(\text{Co}^{\text{II}}(\text{Ch}_n))$  system (b) [45], [copyright 2015 American Chemical Society](#).

In addition to the above work, [an octahedral  \$\text{Cd}\_3\(\text{C}\_3\text{N}\_3\text{S}\_3\)\_2\$  coordination polymer was exploited and Zhuang et al. earlier reported an octahedral  \$\text{Cd}\_3\(\text{C}\_3\text{N}\_3\text{S}\_3\)\_2\$  coordination polymer for enhanced photocatalytic  \$\text{H}\_2\text{O}\_2\$  production from methanol/water solution \[37\] \(Fig. 14 a, b\). Later, the octahedron  \$\text{Cd}\_3\(\text{C}\_3\text{N}\_3\text{S}\_3\)\_2\$  was adhered to the reduced graphene \(rGO\) \(xrGO/ \$\text{Cd}\_3\(\text{TMT}\)\_2\$ \) to become a improved photocatalyst for visible light-driven  \$\text{H}\_2\text{O}\_2\$  production. Later, Xu et al. adhered the octahedron  \$\text{Cd}\_3\(\text{C}\_3\text{N}\_3\text{S}\_3\)\_2\$  to reduced graphene \(rGO\) \[38\]. The formation of  \$\text{H}\_2\text{O}\_2\$  was 2.5-folds enhanced and its deformation was concurrently suppressed. The enhanced performance mainly resulted from the accelerated charge transfer process, which was originated from the supreme electrically conductive properties of graphene.](#)

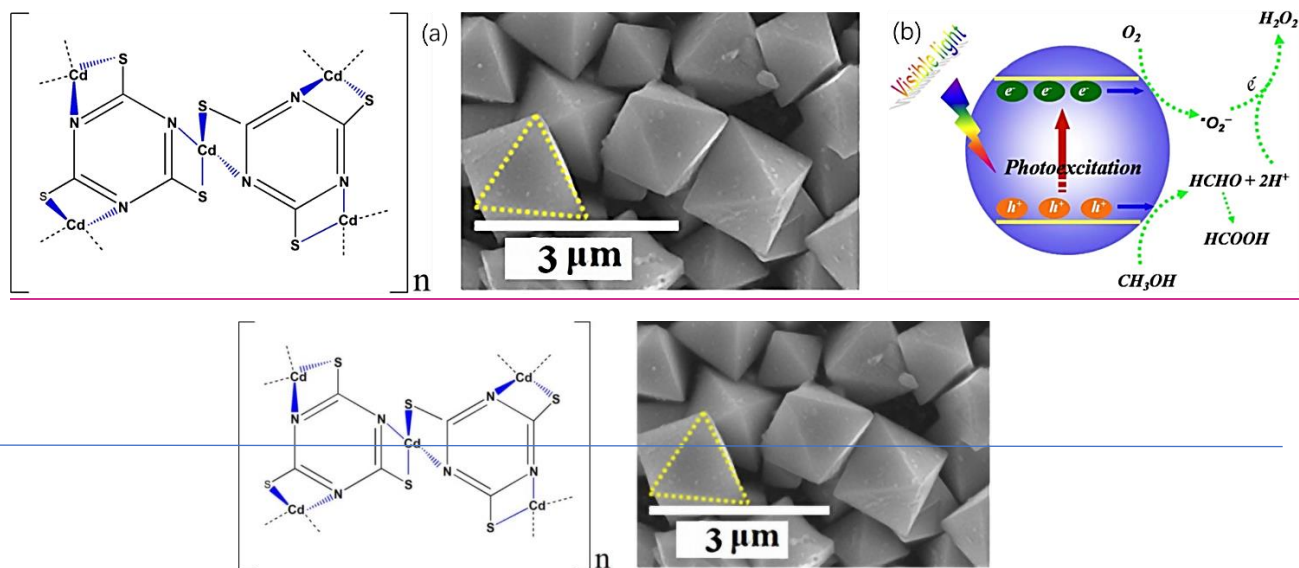


Fig. 14. Structure and SEM image of  $\text{Cd}_3(\text{C}_3\text{N}_3\text{S}_3)_2$  coordination polymer (a), and its photocatalytic  $\text{H}_2\text{O}_2$  production pathway (b) [37], copyright 2015 Nature.

Fig. 14. Structure and SEM image of  $\text{Cd}_3(\text{C}_3\text{N}_3\text{S}_3)_2$  coordination polymer [37].

Transition metal complexes including MOFs materials possess the attractive features that their structures can be modified and regulated from 2D to 3D to achieve desired properties. The transition metal complexes as novel photocatalysts for visible light-driven  $\text{H}_2\text{O}_2$  production can provide appropriate bandgaps and one-electron components to efficiently and selectively promote the two-electron reduction of  $\text{O}_2$  after modification. The unique systems of transition metal complexes are worthy of in-depth studying.

Table 3 Summary of the modification strategies, photocatalytic performances and properties of the reported transition metal complexes for photocatalytic H<sub>2</sub>O<sub>2</sub> production.

<u>Photocatalyst</u>	<u>Modification strategy</u>	<u>Reaction system</u>	<u>H<sub>2</sub>O<sub>2</sub> productivity</u>	<u>Reference</u>
<u>MIL-125-NH<sub>2</sub></u>	<u>Post-synthetic modification with alkyl chains</u>	<u>Visible light; benzylalcohol/water; O<sub>2</sub></u>	<u>2.4 mM (3 h)</u>	<u>[73]</u>
<u>OPA/MIL-125-NH<sub>2</sub></u>	<u>Alkylated process</u>	<u>Visible light; benzylalcohol/water; O<sub>2</sub></u>	<u>6.5 mM (3 h)</u>	<u>[74]</u>
<u>Zn-5-aminoindazole</u>	<u>Pristine</u>	<u>280-360 nm irradiation; water</u>	<u>63 mM/day</u>	<u>[75]</u>
<u>QuPh<sup>+</sup>-NA</u>	<u>-</u>	<u>334 nm irradiation; acetonitrile-water; O<sub>2</sub></u>	<u>36 mM (5 h)</u>	<u>[47]</u>
<u>[Ru(Me<sub>2</sub>phen)<sub>3</sub>]<sup>2+</sup> Ir(OH)<sub>3</sub></u>	<u>-</u>	<u>Visible light; water; O<sub>2</sub></u>	<u>612 μM (9 h)</u>	<u>[43]</u>
<u>[Ru(Me<sub>2</sub>phen)<sub>3</sub>]<sup>2+</sup></u>	<u>-</u>	<u>Visible light; water; O<sub>2</sub></u>	<u>2.0 mM (24 h)</u>	<u>[44]</u>
<u>[Ir(Cp*)(H<sub>2</sub>O)<sub>3</sub>]<sup>2+</sup></u>	<u>-</u>	<u>O<sub>2</sub></u>		
<u>[Ru(Me<sub>2</sub>phen)<sub>3</sub>]<sup>2+</sup></u>	<u>-</u>	<u>Visible light; water with Sc<sup>3+</sup>; O<sub>2</sub></u>	<u>350 μM (15 h)</u>	<u>[41]</u>
<u>Co<sub>3</sub>[Fe(CN)<sub>6</sub>]<sub>2</sub></u>	<u>Template-free</u>	<u>Visible light; 20 mL</u>	<u>8.8 mM (4 h)</u>	<u>[37]</u>

---

<u>Cd<sub>3</sub>(C<sub>3</sub>N<sub>3</sub>S<sub>3</sub>)<sub>2</sub></u>	<u>wet-chemical</u>	<u>methanol/water, pH</u>	
<u>coordination</u>	<u>synthesis</u>	<u>= 2.8</u>	
<u>polymer</u>			
<u>xrGO/Cd<sub>3</sub>(TMT)<sub>2</sub></u>	<u>Stepwise</u>	<u>Visible light; 20 mL</u>	<u>7.2 mM (25 h)</u> [38]
	<u>fabrication</u>	<u>methanol/water; O<sub>2</sub></u>	
	<u>procedures</u>		

---

## 5. Other semiconductor materials

The modification strategies, photocatalytic performances and properties of other semiconductor materials for photocatalytic H<sub>2</sub>O<sub>2</sub> production are collected in Table 4.

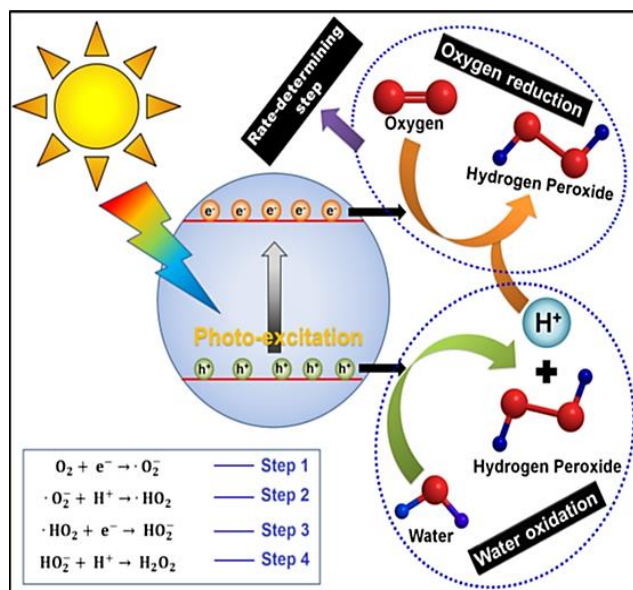
### 5.1. ZnO based materials

ZnO is a type of semiconductor to be earlier reported in the field of photocatalytic H<sub>2</sub>O<sub>2</sub> production. In 1988, Hoffmann's group used ZnO contained illuminated aqueous suspension for photocatalytic H<sub>2</sub>O<sub>2</sub> production in the presence of O<sub>2</sub> and organic electron donors [29]. They proposed that H<sub>2</sub>O<sub>2</sub> could be produced through reduction of O<sub>2</sub> by CB electrons, and the yield of photogenerated CB electrons could be increased by adding electron donors. Later, they used aqueous suspensions of transparent quantum-sized ZnO semiconductor colloids to produce steady-state concentrations of H<sub>2</sub>O<sub>2</sub> as high as 2 mM [76]. The initial rate of H<sub>2</sub>O<sub>2</sub> production was 100-1000 times faster with quantum-sized ZnO than that with bulky ZnO.

### 5.2. Transition metal sulfide-based materials

CdS is employed to be an efficient catalyst since its relatively high CB edge position is advantageous for O<sub>2</sub> reduction and the subsequent H<sub>2</sub>O<sub>2</sub> production. Kim et al. started with silica nanocapsules (SNCs) that host CdS photocatalysts on their shell surfaces to achieve

photocatalytic production of  $\text{H}_2\text{O}_2$  through sensitized triplet-triplet annihilation (TTA) upconversion (UC) of low-energy, sub-bandgap photons. They further loaded a graphene oxide nanodisk (GOND) as a co-catalyst (GOND/CdS-SNC) [36] (~~Fig. 15~~). The photogenerated electrons were efficiently transferred into GOND to retard rapid charge recombination in CdS, which subsequently reduced dioxygen to produce  $\text{H}_2\text{O}_2$  up to a 100 mmol level per hour. Later, a CdS-reduced graphene oxide (RGO) hybrid achieved photocatalytic production of  $\text{H}_2\text{O}_2$  under sunlight from water and  $\text{O}_2$  without using organic electron donors ~~Thakur et al. achieved photocatalytic production of  $\text{H}_2\text{O}_2$  without organic electron donors over a CdS-reduced graphene oxide (RGO) hybrid under sunlight with water and  $\text{O}_2$~~  [35]. The optimal catalyst showed five times of  $\text{H}_2\text{O}_2$  production higher than CdS nanoparticles. Photocatalytic reaction was mainly proceeded by two-electron reduction of  $\text{O}_2$  rather than water oxidation on the catalyst surface. The CB level of CdS was demonstrated to be more negative than the reduction potential of  $\text{O}_2$ , which was sufficient for the high selectivity for the two-electron reduction of  $\text{O}_2$  (Fig. 15). In addition, the photocatalytic system was suitable to be operated at lower temperature and pH.



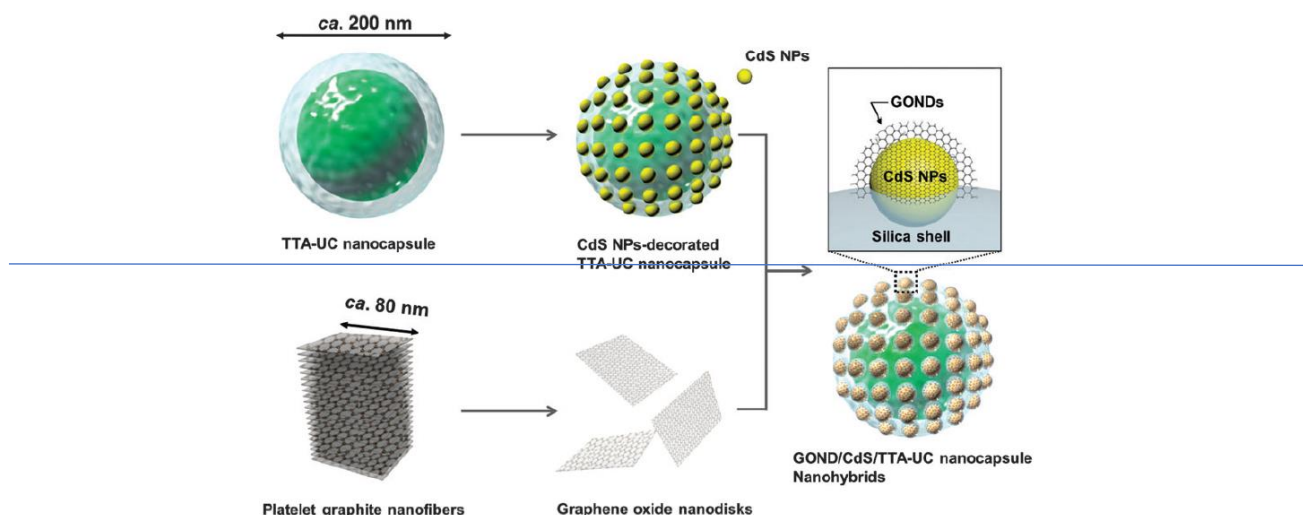


Fig. 15. Plausible mechanism for production of H<sub>2</sub>O<sub>2</sub> by CdS-G hybrid under sunlight [35].

copyright 2017 Elsevier.

Fig. 15. Schematic illustration for the TTA-UC ternary nanohybrid preparation based on the selective GOND wrapping of CdS nanoparticles attached on the surface of TTA-UC nanocapsules [36].

In a recent work of our group, atomic-scale Au modified MoS<sub>2</sub> nanosheets as a photocatalyst for light driven H<sub>2</sub>O<sub>2</sub> production was prepared via a simple pathway including the deposition-reduction and immobilization process [39]. Au modification brought out the low recombination rate of e<sup>-</sup>-h<sup>+</sup> pairs, long lifetime of electrons and more negative flat band potential for MoS<sub>2</sub>. The catalyst achieved efficient photocatalytic production of H<sub>2</sub>O<sub>2</sub> from H<sub>2</sub>O and air in the absence of pure O<sub>2</sub> and organic electron donors. An optimal catalyst enhanced the H<sub>2</sub>O<sub>2</sub> productivity by about 2.5 times based on bare MoS<sub>2</sub>. The H<sub>2</sub>O<sub>2</sub> productivity at pH = 9 was further enhanced by 7.4 times based on that at pH = 2 (Fig. 16).

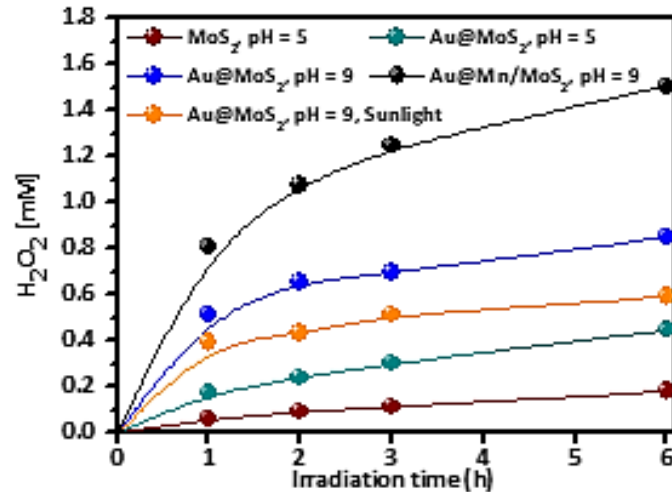


Fig. 16. Photocatalytic H<sub>2</sub>O<sub>2</sub> production over atomic-scale Au modified MoS<sub>2</sub> nanosheets under different conditions [39] [copyright 2019 Elsevier](#).

In recent years, the application potential of transition metal sulfides gradually emerges in the field of photocatalytic H<sub>2</sub>O<sub>2</sub> production. The VB tops of some transition metal sulfides locate at an appropriate range, which provide the strong thermodynamic driving force for water oxidation. In addition, the CB levels of some transition metal sulfides are more negative than the reduction potential of O<sub>2</sub>, which provide enough potential for O<sub>2</sub> reduction. Therefore, it is advised that more sorts of transition metal sulfides can be explored in photocatalytic H<sub>2</sub>O<sub>2</sub> production systems.

### 5.3. Bi containing semiconductors

BiVO<sub>4</sub> loaded with Au nanoparticles was first reported for photocatalytic production of H<sub>2</sub>O<sub>2</sub> in pure water with O<sub>2</sub> ~~Hirakawa et al. reported BiVO<sub>4</sub> loaded with Au nanoparticles for photocatalytic production of H<sub>2</sub>O<sub>2</sub> in pure water with O<sub>2</sub>~~ [40]. The bottom of the BiVO<sub>4</sub> conduction band was more positive than the one-electron reduction potential of O<sub>2</sub> while more negative than the two-electron reduction potential of O<sub>2</sub> (Fig. 17). Therefore, one-electron reduction of O<sub>2</sub> was suppressed and the selectivity for two-electron reduction of O<sub>2</sub> was

promoted, resulting in efficient  $\text{H}_2\text{O}_2$  formation. In a Later work, plasmonic Bi/Bi<sub>2</sub>O<sub>2-x</sub>CO<sub>3</sub> with surface oxygen vacancies was synthesized for photocatalytic production of  $\text{H}_2\text{O}_2$ , and the role of in situ generated  $\text{H}_2\text{O}_2$  for photocatalytic removal of gaseous  $\text{NO}_x$  was investigated ~~Later, Lu et al. reported the role of in situ generated  $\text{H}_2\text{O}_2$  for photocatalytic removal of gaseous  $\text{NO}_x$  [77]. In this work, plasmonic Bi/Bi<sub>2</sub>O<sub>2-x</sub>CO<sub>3</sub> with surface oxygen vacancies was synthesized.~~

In-situ introduction of plasmonic Bi on the surface of Bi<sub>2</sub>O<sub>2-x</sub>CO<sub>3</sub> promoted the generation of  $\text{H}_2\text{O}_2$  at mM scale by capturing electrons from the defect states of Bi<sub>2</sub>O<sub>2-x</sub>CO<sub>3</sub> via the two-electron reduction of  $\text{O}_2$ . The dissociation of  $\text{H}_2\text{O}_2$  was concluded to be interdicted by the in situ formation of Bi, which suppressed the single electron reduction of  $\text{H}_2\text{O}_2$  to  $\cdot\text{OH}$  and enhanced the selectivity of  $\text{O}_2$  reduction to  $\text{H}_2\text{O}_2$ . The presence of oxygen vacancies in Bi/Bi<sub>2</sub>O<sub>2-x</sub>CO<sub>3</sub> was critical to  $\text{H}_2\text{O}_2$  production selectivity. The above two works presented the feasibility of photocatalytic production of  $\text{H}_2\text{O}_2$  over the Bi containing semiconductors.

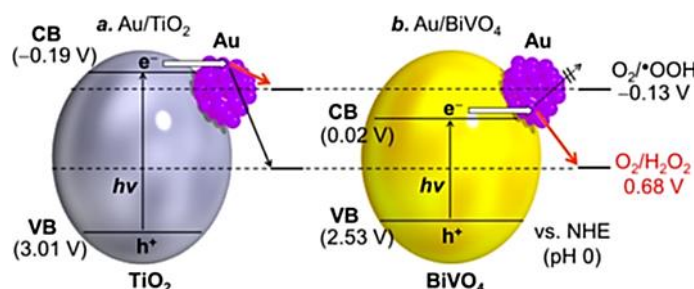


Fig. 17. Energy diagrams for Au/TiO<sub>2</sub> and Au/BiVO<sub>4</sub> and reduction potential of O<sub>2</sub> [40]

copyright 2016 American Chemical Society.

#### 5.4. Carbon materials

Carbon family including graphene nanomaterials are emerging photocatalysts consisting of earth-abundant elements. A carbon dot-impregnated waterborne hyperbranched polyurethane was developed ~~Gogoi et al. developed a carbon dot-impregnated waterborne hyperbranched polyurethane~~ as a heterogeneous photocatalyst for solar driven production of  $\text{H}_2\text{O}_2$  in the



presence of C<sub>2</sub>H<sub>5</sub>OH and O<sub>2</sub> [78]. The carbon dots possessed a suitable bandgap of 2.98 eV, which facilitated effective splitting of both water and ethanol under solar irradiation. In the system, photoreaction of C<sub>2</sub>H<sub>5</sub>OH with H<sub>2</sub>O around room temperature promoted selective H<sub>2</sub>O<sub>2</sub> production. ~~Hou et al. reported that~~ In another report, graphene oxide could efficiently catalyzed photogeneration of H<sub>2</sub>O<sub>2</sub> to mmol levels in the absence of electron donors [20]. ~~They~~ It was found that the dissolved O<sub>2</sub> contributed to the H<sub>2</sub>O<sub>2</sub> generation, and H<sub>2</sub>O<sub>2</sub> photoproduction was readily enhanced by raising pH.

Table 4 Summary of the modification strategies, photocatalytic performances and properties of other materials for photocatalytic H<sub>2</sub>O<sub>2</sub> production.

<u>Photocatalyst</u>	<u>Modification strategy</u>	<u>Reaction system</u>	<u>H<sub>2</sub>O<sub>2</sub> productivity</u>	<u>Reference</u>
<u>GOND/CdS-SNC</u>	<u>Emulsification, sol-gel, exfoliation</u>	<u>Visible light; alcohol/water; O<sub>2</sub></u>	<u>92 μM (1 h)</u>	<u>[36]</u>
<u>CdS-RGO</u>	<u>Hydrothermal method</u>	<u>Sunlight; 50 mL water contained H<sub>2</sub>SO<sub>4</sub>; O<sub>2</sub></u>	<u>128 μM (12 h)</u>	<u>[35]</u>
<u>Atomic Au@MoS<sub>2</sub></u>	<u>Reduction, deposition</u>	<u>Sunlight; 50 mL water, pH = 9</u>	<u>792 μM (6 h)</u>	<u>[39]</u>
<u>Au/BiVO<sub>4</sub></u>	<u>Deposition precipitation</u>	<u>Visible light; 30 mL EtOH/water; O<sub>2</sub></u>	<u>40 μM (10 h)</u>	<u>[40]</u>
<u>Polymer supported</u>	<u>Hydrothermal,</u>	<u>Visible light;</u>	<u>83 μM (50 h)</u>	<u>[78]</u>

---

<u>carbon dots</u>	<u>mechanical,</u>	<u>EtOH/water; O<sub>2</sub></u>		
	<u>ultrasonic</u>			
<u>Graphene oxide</u>	<u>Pristine</u>	<u>Visible light; 7 mL</u>	<u>195 μM (6 h)</u>	[20]
		<u>of GO suspension;</u>		
		<u>O<sub>2</sub></u>		

---

## 6. Summary and outlook

Nowadays, photocatalytic production of H<sub>2</sub>O<sub>2</sub> is becoming a research hotspot, because it exhibits cost-efficient and eco-friendly advantages, and can adapt to the applications of environmental remediation, organic synthesis and fuel cells. This minireview covers most of the advanced catalysts and techniques of H<sub>2</sub>O<sub>2</sub> photoproduction, and highlights the advanced modification strategies for semiconductor catalysts to enhance their H<sub>2</sub>O<sub>2</sub> productivity. So far, various photocatalyst families have been explored, such as ZnO, g-C<sub>3</sub>N<sub>4</sub>, TiO<sub>2</sub>, metal complexes, metal sulfides, Bi containing semiconductors, and carbon materials et al. Modification strategies are mainly classified as structure/morphology modulation, surface decoration, elements doping, and semiconductors hybridization. The modifications mainly aim at increase in the inner space of semiconductors, activation of the molecular O<sub>2</sub>, inhibition of the photocarriers recombination, promotion of the electron transfer, and weakening the photocatalytic H<sub>2</sub>O<sub>2</sub> decomposition. Photocatalytic H<sub>2</sub>O<sub>2</sub> production technique is developing in a challenging stage, and thus it has huge space to become mature. The technique still faces the issues that the H<sub>2</sub>O<sub>2</sub> productivity is expected to be increased into a higher scale, the use of electron donors and pure O<sub>2</sub> should be lowered, the selectivity of two-electron reduction of O<sub>2</sub> requires to be further increased over one- or four-electron reduction of O<sub>2</sub>. The fundamental

solution of all the issues is to explore more efficient semiconductor catalysts, as well as their synthesis and modification strategies. The key avenues should focus on modulating the electron structure of semiconductors, suppressing the decomposition of as-prepared H<sub>2</sub>O<sub>2</sub>, and enhancing the activation and utilization of O<sub>2</sub>. Moreover, the mechanisms of various photocatalytic H<sub>2</sub>O<sub>2</sub> production systems are also necessary to be investigated in depth to design and optimize the photocatalysts with high efficiency. In this regard, researchers may employ high-efficiency characterization methods to study the morphology and photoelectric properties of photocatalysts, and use theory calculation approaches to design and study the photocatalytic H<sub>2</sub>O<sub>2</sub> production system. We expect that the photocatalytic H<sub>2</sub>O<sub>2</sub> production is now in progress along with more and more novel synthetic strategies of photocatalyst and improved procedures.

## **Acknowledgements**

This project was supported by Heilongjiang Provincial Natural Science Foundation of China (LH2019B023), the China Postdoctoral Science Foundation funded project (2016M601403), and the Scientific Research Project of Harbin Institute of Petroleum (HIPJJ201917).

## **References**

1. Sato K, Aoki M, Noyori R (1998) A "Green" route to adipic acid: Direct oxidation of cyclohexenes with 30 percent hydrogen peroxide. *Science* 281:1646-1647.
2. Niwa S-i, Eswaramoorthy M, Nair J, Raj A, Itoh N, Shoji H, Namba T, Mizukami F (2002) A one-step conversion of benzene to phenol with a palladium membrane. *Science* 295:105-107.
3. Shaegh SAM, Nguyen N-T, Ehteshamiab SMM, Chan SH (2012) A membraneless hydrogen

peroxide fuel cell using Prussian Blue as cathode material. *Energy Environ. Sci.* 5:8225-8228.

4. Fukuzumi S (2017) Production of liquid solar fuels and their use in fuel cells. *Joule* 1:689-738.

5. Fukuzumi S (2016) Artificial photosynthesis for production of hydrogen peroxide and its fuel cells. *Biochim. Biophys. Acta* 1857:604-611.

6. Campos-Martin JM, Blanco-Brieva G, Fierro JLG (2006) Hydrogen peroxide synthesis: An outlook beyond the anthraquinone process. *Angew. Chem. Int. Ed.* 45:6962-6984.

7. Hou H, Zeng X, Zhang X Production of hydrogen peroxide through photocatalytic processes: a critical review of recent advances. *Angew. Chem. Int. Ed.* doi.org/10.1002/anie.201911609:

8. Sheldon RA, Arends IWCE (2004) Organocatalytic oxidations mediated by nitroxyl radicals. *Adv. Synth. Catal.* 346:1051-1071.

9. Foller PC, Bombard RT (1995) Processes for the production of mixtures of caustic soda and hydrogen peroxide via the reduction of oxygen. *J. Appl. Electrochem.* 25:613-627.

10. Edwards JK, Solsona BE, Landon P, Carley AF, Herzing A, Kiely CJ, Hutchings GJ (2005) Direct synthesis of hydrogen peroxide from H<sub>2</sub> and O<sub>2</sub> using TiO<sub>2</sub>-supported Au-Pd catalysts. *J. Catal.* 236:69-79.

11. Song H, Li G, Wang X, Chen Y (2011) Characterization and catalytic performance of Au/Ti-HMS for direct generation of H<sub>2</sub>O<sub>2</sub> and in situ-H<sub>2</sub>O<sub>2</sub>-ODS from H<sub>2</sub> and O<sub>2</sub>: An in situ-reduction synthesis and a recycle study of catalyst. *Micropor. Mesopor. Mat.* 139:104-109.

12. Edwards JK, Solsona B, N EN, Carley AF, Herzing AA, Kiely CJ, Hutchings GJ (2009) Switching off hydrogen peroxide hydrogenation in the direct synthesis process. *Science* 323:1037-1041.

13. Edwards JK, Solsona BE, Landon P, Carley AF, Herzing A, Kiely CJ, Hutchings GJ (2005) Direct synthesis of hydrogen peroxide from H<sub>2</sub> and O<sub>2</sub> using TiO<sub>2</sub>-supported Au-Pd catalysts. *J. Catal.* 236:69-79.
14. Edwards JK, Pritchard J, Piccinini M, Shaw G, He Q, Carley AF, Kiely CJ, Hutchings GJ (2012) The effect of heat treatment on the performance and structure of carbon-supported Au-Pd catalysts for the direct synthesis of hydrogen peroxide. *J. Catal.* 292:227-238.
15. Henkel H, Weber W (Henkel & CIE) (1914) US1108752 [Chem. Abstr. 1914, 8, 23927].
16. Li S, Dong G, Hailili R, Yang L, Li Y, Wang F, Zeng Y, Wang C (2016) Effective photocatalytic H<sub>2</sub>O<sub>2</sub> production under visible light irradiation at g-C<sub>3</sub>N<sub>4</sub> modulated by carbon vacancies. *Appl. Catal. B: Environ.* 190:26-35.
17. Baur E, Neuweiler C (1927) Photolytic formation of hydrogenperoxide. *Helv, Chim. Acta* 10:901-907.
18. Yang L, Dong G, Jacobs DL, Wang Y, Zang L, Wang C (2017) Two-channel photocatalytic production of H<sub>2</sub>O<sub>2</sub> over g-C<sub>3</sub>N<sub>4</sub> nanosheets modified with perylene imides. *J. Catal.* 352:274-281.
19. Zhu Z, Pan H, Muruganathan M, Gong J, Zhang Y (2018) Visible light-driven photocatalytically active g-C<sub>3</sub>N<sub>4</sub> material for enhanced generation of H<sub>2</sub>O<sub>2</sub>. *Appl. Catal. B: Environ.* 232:19-25.
20. Hou W-C, Wang Y-S (2017) Photocatalytic generation of H<sub>2</sub>O<sub>2</sub> by graphene oxide in organic electron donor-free condition under sunlight. *ACS Sustainable Chem. Eng.* 5:2994-3001.
21. Shiraishi Y, Kanazawa S, Sugano Y, Tsukamoto D, Sakamoto H, Ichikawa S, Hirai T (2014) Highly selective production of hydrogen peroxide on graphitic carbon nitride (g-C<sub>3</sub>N<sub>4</sub>)

photocatalyst activated by visible light. *ACS Catal.* 4:774-780.

22. Shiraishi Y, Kanazawa S, Kofuji Y, Sakamoto H, Ichikawa S, Tanaka S, Hirai T (2014) Sunlight-driven hydrogen peroxide production from water and molecular oxygen by metal-free photocatalysts. *Angew. Chem. Int. Ed.* 53:13454-13459.

23. Zhao S, Zhao X, Zhang H, Li J, Zhu Y (2017) Covalent combination of polyoxometalate and graphitic carbon nitride for light-driven hydrogen peroxide production. *Nano Energy* 35:405-414.

24. Hu S, Qu X, Li P, Wang F, Li Q, Song L, Zhao Y, Kang X (2018) Photocatalytic oxygen reduction to hydrogen peroxide over copper doped graphitic carbon nitride hollow microsphere: The effect of Cu(I)-N active sites. *Chem. Eng. J.* 334:410-418.

25. Kofuji Y, Ohkita S, Shiraishi Y, Sakamoto H, Tanaka S, Ichikawa S, Hirai T (2016) Graphitic carbon nitride doped with biphenyl diimide: Efficient photocatalyst for hydrogen peroxide production from water and molecular oxygen by sunlight. *ACS Catal.* 6:7021-7029.

26. Shiraishi Y, Kofuji Y, Sakamoto H, Tanaka S, Ichikawa S, Hirai T (2015) Effects of surface defects on photocatalytic H<sub>2</sub>O<sub>2</sub> production by mesoporous graphitic carbon nitride under visible light irradiation. *ACS Catal.* 5:3058-3066.

27. Zhao S, Guo T, Li X, Xue T, Yang B, Zhao X (2018) Carbon nanotubes covalent combined with graphitic carbon nitride for photocatalytic hydrogen peroxide production under visible light. *Appl. Catal. B: Environ.* 224:725-732.

28. Kim S, Moon G-h, Kim H, Mun Y, Zhang P, Lee J, Choi W (2018) Selective charge transfer to dioxygen on KPF<sub>6</sub>-modified carbon nitride for photocatalytic synthesis of H<sub>2</sub>O<sub>2</sub> under visible light. *J. Catal.* 357:51-58.

29. Kormann C, Bahnemann DW, Hoffmann MR (1988) Photocatalytic production of H<sub>2</sub>O<sub>2</sub> and organic peroxides in aqueous suspensions of TiO<sub>2</sub>, ZnO, and desert sand. *Environ. Sci. Technol.* 22:798-806.
30. Tsukamoto D, Shiro A, Shiraishi Y, Sugano Y, Ichikawa S, Tanaka S, Hirai T (2012) Photocatalytic H<sub>2</sub>O<sub>2</sub> production from ethanol/O<sub>2</sub> system using TiO<sub>2</sub> loaded with Au-Ag bimetallic alloy nanoparticles. *ACS Catal.* 2:599-603.
31. Shiraishi Y, Kanazawa S, Tsukamoto D, Shiro A, Sugano Y, Hirai T (2013) Selective hydrogen peroxide formation by titanium dioxide photocatalysis with benzylic alcohols and molecular oxygen in water. *ACS Catal.* 3:2222-2227.
32. Moon G-h, Kim W, Bokare AD, Sung N-e, Choi W (2014) Solar production of H<sub>2</sub>O<sub>2</sub> on reduced graphene oxide-TiO<sub>2</sub> hybrid photocatalysts consisting of earth-abundant elements only. *Energy Environ. Sci.* 7:4023-4028.
33. Bandara J, Udawatta CPK, Rajapakse CSK (2005) Highly stable CuO incorporated TiO<sub>2</sub> catalyst for photocatalytic hydrogen production from H<sub>2</sub>O. *Photochem. Photobiol. Sci.* 4:857-861.
34. Maurino V, Minero C, Mariella G, Pelizzetti E (2005) Sustained production of H<sub>2</sub>O<sub>2</sub> on irradiated TiO<sub>2</sub>-fluoride systems *Chem. Commun.* 2627-2629.
35. Thakur S, Kshetri T, Kim NH, Lee JH (2017) Sunlight-driven sustainable production of hydrogen peroxide using a CdS-graphene hybrid photocatalyst. *J. Catal.* 345:78-86.
36. Kim H-i, Kwon OS, Kim S, Choi W, Kim J-H (2016) Harnessing low energy photons (635 nm) for the production of H<sub>2</sub>O<sub>2</sub> using upconversion nanohybrid photocatalysts. *Energy Environ. Sci.* 9:1063-1073.

37. Zhuang H, Yang L, Xu J, Li F, Zhang Z, Lin H, Long J, Wang X (2015) Robust photocatalytic H<sub>2</sub>O<sub>2</sub> production by octahedral Cd<sub>3</sub>(C<sub>3</sub>N<sub>3</sub>S<sub>3</sub>)<sub>2</sub> coordination polymer under visible light. *Sci. Rep.* 5:16947.
38. Xu J, Chen Z, Zhang H, Lin G, Lin H, Wang X, Long J (2017) Cd<sub>3</sub>(C<sub>3</sub>N<sub>3</sub>S<sub>3</sub>)<sub>2</sub> coordination polymer/graphene nanoarchitectures for enhanced photocatalytic H<sub>2</sub>O<sub>2</sub> production under visible light. *Sci. Bull.* 62:610-618.
39. Song H, Wei L, Chen C, Wen C, Han F (2019) Photocatalytic production of H<sub>2</sub>O<sub>2</sub> and its in situ utilization over atomic-scale Au modified MoS<sub>2</sub> nanosheets. *J. Catal.* 376:198-208.
40. Hirakawa H, Shiota S, Shiraishi Y, Sakamoto H, Ichikawa S, Hirai T (2016) Au nanoparticles supported on BiVO<sub>4</sub>: Effective inorganic photocatalysts for H<sub>2</sub>O<sub>2</sub> production from water and O<sub>2</sub> under visible light. *ACS Catal.* 6:4976-4982.
41. Isaka Y, Oyama K, Yamada Y, Suenobu T, Fukuzumi S (2016) Photocatalytic production of hydrogen peroxide from water and dioxygen using cyano-bridged polynuclear transition metal complexes as water oxidation catalysts. *Catal. Sci. Technol.* 6:681-684.
42. Mase K, Yoneda M, Yamada Y, Fukuzumi S (2016) Efficient photocatalytic production of hydrogen peroxide from water and dioxygen with bismuth vanadate and a cobalt(II) chlorin complex. *ACS Energy Lett.* 1:913-919.
43. Kato S, Jung J, Suenobu T, Fukuzumi S (2013) Production of hydrogen peroxide as a sustainable solar fuel from water and dioxygen. *Energy Environ. Sci.* 6:3756-3764.
44. Isaka Y, Kato S, Hong D, Suenobu T, Yamada Y, Fukuzumi S (2015) Bottom-up and top-down methods to improve catalytic reactivity for photocatalytic production of hydrogen peroxide using a Ru-complex and water oxidation catalysts. *J. Mater. Chem. A* 3:12404-12412.



45. Mase K, Ohkubo K, Fukuzumi S (2015) Much enhanced catalytic reactivity of cobalt chlorin derivatives on two-electron reduction of dioxygen to produce hydrogen peroxide. *Inorg. Chem.* 54:1808-1815.
46. Yamada Y, Nomura A, Miyahigashia T, Fukuzumi S (2012) Photocatalytic production of hydrogen peroxide by two-electron reduction of dioxygen with carbon-neutral oxalate using a 2-phenyl-4-(1-naphthyl)quinolinium ion as a robust photocatalyst. *Chem. Commun.* 48:8329-8331.
47. Yamada Y, Nomura A, Miyahigashi T, Ohkubo K, Fukuzumi S (2013) Acetate induced enhancement of photocatalytic hydrogen peroxide production from oxalic acid and dioxygen. *J. Phys. Chem. A* 117:3751-3760.
48. Shiraishi Y, Kanazawa S, Kofuji Y, Sakamoto H, Ichikawa S, Tanaka S, Hirai T (2014) Sunlight-driven hydrogen peroxide production from water and molecular oxygen by metal-free photocatalysts. *Angew. Chem. Int. Ed.* 53:1-7.
49. Ou H, Yang P, Lin L, Anpo M, Wang X (2017) Carbon nitride aerogels for the photoredox conversion of water. *Angew. Chem. Int. Ed.* 56:10905-10910.
50. Li S, Dong G, Hailili R, Yang L, Li Y, Wang F, Zeng Y, Wang C (2016) Effective photocatalytic H<sub>2</sub>O<sub>2</sub> production under visible light irradiation at g-C<sub>3</sub>N<sub>4</sub> modulated by carbon vacancies. *Appl. Catal. B: Environ.* 190:26-35.
51. Lu N, Liu N, Hui Y, Shang K, Jiang N, Li J, YanWu (2020) Characterization of highly effective plasma-treated g-C<sub>3</sub>N<sub>4</sub> and application to the photocatalytic H<sub>2</sub>O<sub>2</sub> production. *Chemosphere* 241:124927.
52. Moon G-h, Fujitsuka M, Kim S, Majima T, Wang X, Choi W (2017) Eco-friendly

photochemical production of H<sub>2</sub>O<sub>2</sub> through O<sub>2</sub> reduction over carbon nitride frameworks incorporated with multiple heteroelements. *ACS Catal.* 7:2886-2895.

53. Tian J, Wu T, Wang D, Pei Y, Qiao M, Zong B (2019) One-pot synthesis of potassium and phosphorus-doped carbon nitride catalyst derived from urea for highly efficient visible light-driven hydrogen peroxide production. *Catal. Today* 330:171-178.

54. Xue F, Si Y, Wang M, Liu M, Guo L (2019) Toward efficient photocatalytic pure water splitting for simultaneous H<sub>2</sub> and H<sub>2</sub>O<sub>2</sub> production. *Nano Energy* 62:823-831.

55. Teranishi M, Naya S-i, Tada H (2010) In situ liquid phase synthesis of hydrogen peroxide from molecular oxygen using gold nanoparticle-loaded titanium(IV) dioxide photocatalyst. *J. Am. Chem. Soc.* 132:7850-7851.

56. Zuo G, Liu S, Wang L, Song H, Zong P, Hou W, Li B, Guo Z, Meng X, Du Y, Wang T, Roye VAL (2019) Finely dispersed Au nanoparticles on graphitic carbon nitride as highly active photocatalyst for hydrogen peroxide production. *Catal. Commun.* 123:69-72.

57. Yang Y, Zhang C, Huang D, Zeng G, Huang J, Lai C, Zhou C, Wang W, Guo H, Xue W, Deng R, Cheng M, Xiong W (2019) Boron nitride quantum dots decorated ultrathin porous g-C<sub>3</sub>N<sub>4</sub>: Intensified exciton dissociation and charge transfer for promoting visible-light-driven molecular oxygen activation. *Appl. Catal. B: Environ.* 245:87-99.

58. Li H, Pang S, Feng X, Müllen K, Bubeck C (2010) Polyoxometalate assisted photoreduction of graphene oxide and its nanocomposite formatio. *Chem. Commun.* 46:6243-6245.

59. Ma H, Li C, Yin J, Pu X, Zhang D, Su C, Wang X, Shao X (2016) Polyoxometalate enhances the photocatalytic performance of polyaniline/SnO<sub>2</sub> composites. *Mater. Lett.* 168:103-106.

60. Zhao S, Zhao X (2019) Insights into the role of singlet oxygen in the photocatalytic

hydrogen peroxide production over polyoxometalates-derived metal oxides incorporated into graphitic carbon nitride framework. *Appl. Catal. B: Environ.* 250:408-418.

61. Fu Y, Liu Ca, Zhang M, Zhu C, Li H, Wang H, Song Y, Huang H, Liu Y, Kang Z (2018) Photocatalytic H<sub>2</sub>O<sub>2</sub> and H<sub>2</sub> generation from living *Chlorella vulgaris* and carbon micro particle comodified g-C<sub>3</sub>N<sub>4</sub>. *Adv. Energy Mater.* 8:1802525.

62. Wang X, Han Z, Yu L, Liu C, Liu Y, Wu G (2018) Synthesis of full-spectrum-response Cu<sub>2</sub>(OH)PO<sub>4</sub>/g-C<sub>3</sub>N<sub>4</sub> photocatalyst with outstanding photocatalytic H<sub>2</sub>O<sub>2</sub> production performance via a "two channel route". *ACS Sustainable Chem. Eng.* 6:14542-14553.

63. Yang Y, Zeng Z, Zeng G, Huang D, Xiao R, Zhang C, Zhou C, Xiong W, Wang W, Cheng M, Xue W, Guo H, Tang X, He D (2019) Ti<sub>3</sub>C<sub>2</sub> Mxene/porous g-C<sub>3</sub>N<sub>4</sub> interfacial Schottky junction for boosting spatial charge separation in photocatalytic H<sub>2</sub>O<sub>2</sub> production. *Appl. Catal. B: Environ.* 258:117956.

64. Haider Z, Cho H-i, Moon G-h, Kim H-i (2019) Minireview: Selective production of hydrogen peroxide as a clean oxidant over structurally tailored carbon nitride photocatalysts. *Catal. Today* 335:55-64.

65. Cai R, Kubota Y, Fujishima A (2003) Effect of copper ions on the formation of hydrogen peroxide from photocatalytic titanium dioxide particles. *J. Catal.* 219:214-218.

66. Maurino V, Minero C, Pelizzetti E, Mariella G, Arbezano A, Rubertelli F (2007) Influence of Zn(II) adsorption on the photocatalytic activity and the production of H<sub>2</sub>O<sub>2</sub> over irradiated TiO<sub>2</sub>. *Res. Chem. Intermed.* 33:319-332.

67. Wang L, Cao S, Guo K, Wu Z, Ma Z, Piao L (2019) Simultaneous hydrogen and peroxide production by photocatalytic water splitting. *Chinese J. Catal.* 40:470-475.

68. Chu C, Huang D, Zhu Q, Stavitski E, Spies JA, Pan Z, Mao J, Xin HL, Schmuttenmaer CA, Hu S, Kim J-H (2019) Electronic tuning of metal nanoparticles for highly efficient photocatalytic hydrogen peroxide production. *ACS Catal.* 9:626-631.
69. Kim K, Park J, Kim H, Jung GY, Kim M-G (2019) Solid-phase photocatalysts: Physical vapor deposition of Au nanoislands on porous TiO<sub>2</sub> films for millimolar H<sub>2</sub>O<sub>2</sub> production within a few minutes. *ACS Catal.* 9:9206-9211.
70. Zheng L, Su H, Zhang J, Walekar LS, Molamahmood HV, Zhou B, Long M, Hua YH (2018) Highly selective photocatalytic production of H<sub>2</sub>O<sub>2</sub> on sulfur and nitrogen co-doped graphene quantum dots tuned TiO<sub>2</sub>. *Appl. Catal. B: Environ.* 239:475-484.
71. Zheng L, Zhang J, Hu YH, Long M (2019) Enhanced photocatalytic production of H<sub>2</sub>O<sub>2</sub> by nafion coatings on S, N-codoped graphene-quantum-dots-modified TiO<sub>2</sub>. *J. Phys. Chem. C* 123:13693-13701.
72. Ma R, Wang L, Wang H, Liu Z, Xing M, Zhu L, Meng X, Xiao F-S (2019) Solid acids accelerate the photocatalytic hydrogen peroxide synthesis over a hybrid catalyst of titania nanotube with carbon dot. *Appl. Catal. B: Environ.* 244:594-603.
73. Isaka Y, Kawase Y, Kuwahara Y, Mori K, Yamashita H (2019) Two-phase system utilizing hydrophobic metal-organic frameworks (MOFs) for photocatalytic synthesis of hydrogen peroxide. *Angew. Chem. Int. Ed.* 58:5402-5406.
74. Kawase Y, Isaka Y, Kuwahara Y, Mori K, Yamashita H (2019) Ti cluster-alkylated hydrophobic MOFs for photocatalytic production of hydrogen peroxide in two-phase systems. *Chem. Commun.* 55:6743-6746.
75. Hayes JA, Schubert DM, Amonette JE, Nachimuthu P, Disselkamp RS (2008) Ultraviolet

stimulation of hydrogen peroxide production using aminoindazole, diaminopyridine, and phenylenediamine solid polymer complexes of Zn(II). *J. Photoch. Photobio. A Chem.* 197:245-252.

76. Hoffman AJ, Carraway ER, Hoffmann MR (1994) Photocatalytic production of H<sub>2</sub>O<sub>2</sub> and organic peroxides on quantum-sized semiconductor colloids. *Environ. Sci. Technol.* 28:776-785.

77. Lu Y, Huang Y, Zhang Y, Huang T, Li H, Cao J-j, Ho W (2019) Effects of H<sub>2</sub>O<sub>2</sub> generation over visible light-responsive Bi/Bi<sub>2</sub>O<sub>2-x</sub>CO<sub>3</sub> nanosheets on their photocatalytic NO<sub>x</sub> removal performance. *Chem. Eng. J.* 363:374-382.

78. Gogoi S, Karak N (2017) Solar-driven hydrogen peroxide production using polymer-supported carbon dots as heterogeneous catalyst. *Nano-Micro Lett.* 9:40.